

A shifted boundary method based on extension operators

Original

A shifted boundary method based on extension operators / Zorrilla, R., Rossi, R., Scovazzi, G., Canuto, C., Rodríguez-Ferran, A.. - In: COMPUTER METHODS IN APPLIED MECHANICS AND ENGINEERING. - ISSN 0045-7825. - 421:(2024), pp. 1-23. [10.1016/j.cma.2024.116782]

Availability:

This version is available at: 11583/2995183 since: 2024-12-11T10:34:05Z

Publisher:

Elsevier

Published

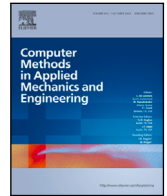
DOI:10.1016/j.cma.2024.116782

Terms of use:

This article is made available under terms and conditions as specified in the corresponding bibliographic description in the repository

Publisher copyright

(Article begins on next page)



A shifted boundary method based on extension operators

Rubén Zorrilla ^{a,b,*}, Riccardo Rossi ^{a,b}, Guglielmo Scovazzi ^c, Claudio Canuto ^d, Antonio Rodríguez-Ferran ^{a,e}

^a Departament d'Enginyeria Civil i Ambiental, Universitat Politècnica de Catalunya, Barcelona, 08034, Spain

^b International Center for Numerical Methods in Engineering (CIMNE), Barcelona, 08034, Spain

^c Department of Civil and Environmental Engineering, Duke University, Durham, NC 27708, USA

^d Dipartimento di Scienze Matematiche, Politecnico di Torino, Torino, 10129, Italy

^e Laboratori de Càlcul Numèric (LaCàN), Universitat Politècnica de Catalunya, Barcelona, 08034, Spain

ARTICLE INFO

Keywords:

Shifted boundary method
Immersed boundary method
Small cut-cell problem
Approximate domain boundaries
Weak boundary conditions
Unfitted finite element methods

ABSTRACT

We consider formulations of the Shifted Boundary Method based on extrapolation operators other than the Taylor expansion. In the specific case of the Poisson equation, we prove that this approach is stable, provided some basic properties of well-posedness of the extrapolation operator are verified.

1. Introduction

When computational mechanics problems involve complex geometries or geometries that are described in non-canonical formats (i.e., STL geometric representations, etc.), the pre-processing phase of cleaning the geometry from spurious artifacts and generating the computational grid may require an overwhelming part of the design and analysis cycle (up to 70%–90%).

In this context, immersed/embedded/unfitted computational methods may provide a more flexible approach to computing, as they do not require fitting the grid to the geometrical features of the shapes to be simulated. In this class of methods are the Immersed Boundary Finite Element Method (IBFEM) [1], the cut Finite Element Method (cutFEM) [2–18], the Finite Cell Method [19,20], and related earlier and recent methods [21–25].

Most of these approaches require the geometric construction of the partial elements cut by the embedded boundary, which can be both algorithmically complicated and computationally intensive, due to data structures that are considerably more complex with respect to corresponding fitted finite element methods. Furthermore, integrating the variational forms on the characteristically irregular cut cells may also be difficult and advanced quadrature formulas might need to be employed [19,20].

The Shifted Boundary Method (SBM) was proposed in [26] as an alternative to existing embedded/unfitted boundary methods and belongs to the more specific class of approximate domain methods [27–35]. Specifically, the SBM was proposed in [26] for the Poisson and Stokes flow problems and generalized in [36] to the advection–diffusion and Navier–Stokes equations, and in [37] to hyperbolic conservation laws. An analysis of the stability and accuracy of the SBM for the Poisson, advection–diffusion, and Stokes operators was also included in [26,36,38], respectively. A high-order version of the SBM was proposed in [39] with a traditional Nitsche penalty stabilization and in [40] without penalties. Applications to solid and fracture mechanics problems were presented in [41–45] and simulations of static and moving interfaces were developed in [46,47].

* Corresponding author at: Departament d'Enginyeria Civil i Ambiental, Universitat Politècnica de Catalunya, Barcelona, 08034, Spain.

E-mail addresses: rzorrilla@cimne.upc.edu (R. Zorrilla), rrossi@cimne.upc.edu (R. Rossi), guglielmo.scovazzi@duke.edu (G. Scovazzi), claudio.canuto@polito.it (C. Canuto), antonio.rodriguez-ferran@upc.edu (A. Rodríguez-Ferran).

<https://doi.org/10.1016/j.cma.2024.116782>

Received 22 July 2023; Received in revised form 10 November 2023; Accepted 14 January 2024

0045-7825/© 2024 The Author(s). Published by Elsevier B.V. This is an open access article under the CC BY license (<http://creativecommons.org/licenses/by/4.0/>).

The SBM is built for minimal computational complexity and does not contain any cut cell by design. In fact, the location where boundary conditions are applied is *shifted* from the true to an approximate (surrogate) boundary, and, at the same time, modified (*shifted*) boundary conditions are applied in order to avoid a reduction in the convergence rates of the overall formulation. In particular, if the boundary conditions associated to the true domain are not appropriately modified on the surrogate domain, only first-order convergence is to be expected.

In the original version of the SBM, the shifted boundary conditions are defined by means of Taylor expansions and are applied weakly, using Nitsche's method, leading to a simple, robust, accurate and efficient algorithm.

However, a Taylor expansion is not the only option to construct a shift in boundary conditions and we consider here an alternative approach.

The new extension operators we develop in this work are in the general class of extrapolation operators based on clouds of sampling points (e.g., *moving least squares*, *gradient reconstruction*, etc.) and are more naturally applicable when the SBM is paired with meshfree/meshless Galerkin approximations [41].

Polynomial extension operators have been applied very recently by Burman et al. in [48] as an alternative to ghost penalties in cutFEMs. In these developments, integration over cut cells of the governing equations was still performed. Our extension operators, instead, are used in combination with the shifted boundary concept to completely avoid integration over cut cells.

Using these new concepts, we derive a Nitsche-type variational formulation and we develop its analysis of stability and convergence, for the Poisson problem with Dirichlet boundary conditions.

A series of computational experiments is presented last, for both the Poisson and linear elasticity equations, including both Dirichlet and Neumann boundary conditions.

This article is organized as follows: Section 2 introduces the general SBM notation; the SBM variational formulation for the Poisson problem is presented in Section 3; the SBM variational formulation for the compressible elasticity equations is developed in Section 4; the definition and properties of the extension operators are discussed in Section 5; the numerical analysis of stability and convergence (for the Poisson problem) is provided in Section 6; numerical tests are presented in Section 7; and, finally, conclusions are summarized in Section 8.

2. Overview of the shifted boundary method (without Taylor expansions)

Notation. Throughout the paper, we will denote by $L^2(\Omega)$ the space of square integrable functions on Ω . We will use the Sobolev spaces $H^m(\Omega) = W^{m,2}(\Omega)$ of index of regularity $m \geq 0$ and index of summability 2, equipped with the (scaled) norm

$$\|v\|_{H^m(\Omega)} = \left(\|v\|_{L^2(\Omega)}^2 + \sum_{k=1}^m \|l(\Omega)^k \mathbf{D}^k v\|_{L^2(\Omega)}^2 \right)^{1/2}, \quad (1)$$

where \mathbf{D}^k is the k th-order spatial derivative operator and $l(A) = \text{meas}_{n_d}(A)^{1/n_d}$ is a characteristic length of the domain A ($n_d = 2, 3$ indicates the number of spatial dimensions). Note, in particular, that $H^0(\Omega) = L^2(\Omega)$. As usual, we use a simplified notation for norms and semi-norms, i.e., we set $\|v\|_{m,\Omega} = \|v\|_{H^m(\Omega)}$ and $|v|_{k,\Omega} = \|l(\Omega)^k \mathbf{D}^k v\|_{0,\Omega} = \|l(\Omega)^k \mathbf{D}^k v\|_{L^2(\Omega)}$.

2.1. The true domain, the surrogate domain and maps

Let Ω be a connected open set in \mathbb{R}^{n_d} with Lipschitz boundary. We consider a closed domain \mathcal{D} such that $\text{clos}(\Omega) \subseteq \mathcal{D}$ and we introduce a family \mathcal{T}_h of admissible and shape-regular triangulations of \mathcal{D} . Then, we restrict each triangulation by selecting those elements that are *fully* contained in $\text{clos}(\Omega)$, i.e., we form the *inner triangulation*

$$\tilde{\mathcal{T}}_h := \{T \in \mathcal{T}_h : T \subset \text{clos}(\Omega)\},$$

which identifies the *surrogate domain*

$$\tilde{\Omega}_h := \text{int} \left(\bigcup_{T \in \tilde{\mathcal{T}}_h} T \right) \subseteq \Omega,$$

with *surrogate boundary* $\tilde{\Gamma}_h := \partial \tilde{\Omega}_h$. We also denote by $\tilde{\mathbf{n}}$ the outward-oriented unit normal vector to $\tilde{\Gamma}_h$. Obviously, $\tilde{\mathcal{T}}_h$ is an admissible and shape-regular triangulation of $\tilde{\Omega}_h$ (see Fig. 1). For reasons that will appear clear in what follows, it is also useful to define the *outer triangulation*

$$\hat{\mathcal{T}}_h := \{T \in \mathcal{T}_h : T \subset \text{clos}(\mathcal{D} \setminus \Omega)\}, \quad (2)$$

and the corresponding *outer (inactive) domain*

$$\hat{\Omega}_h := \text{int} \left(\bigcup_{T \in \hat{\mathcal{T}}_h} T \right) \subseteq \mathcal{D} \setminus \Omega, \quad (3)$$

with boundary $\hat{\Gamma}_h$ (the orange polygonal line in Fig. 1). The classical SBM relies on the construction of a map

$$\mathbf{M}_h : \tilde{\Gamma}_h \rightarrow \Gamma,$$

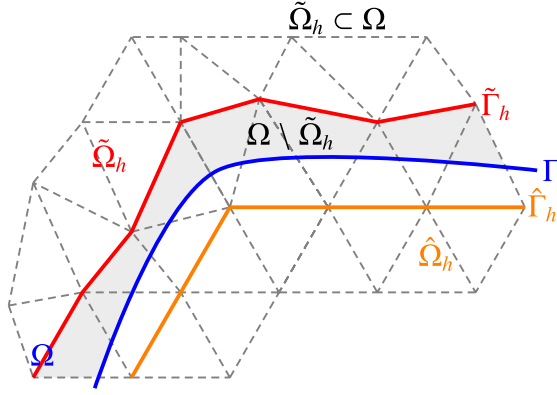


Fig. 1. The true domain Ω and its boundary Γ , the surrogate domain $\tilde{\Omega}_h \subset \Omega$ and its boundary $\tilde{\Gamma}_h$, the outer surrogate domain $\hat{\Omega}_h$ and its boundary $\hat{\Gamma}_h$.

$$\tilde{x} \mapsto \mathbf{x},$$

which associates a point $\mathbf{x} = \mathbf{M}_h(\tilde{\mathbf{x}})$ on the physical boundary Γ to any point $\tilde{\mathbf{x}}$ on the surrogate boundary $\tilde{\Gamma}_h$ [49]. Through \mathbf{M}_h , a distance vector function $\mathbf{d}_{\mathbf{M}_h}$ can be defined as the difference $\mathbf{d}_{\mathbf{M}_h}(\tilde{\mathbf{x}}) = \mathbf{x} - \tilde{\mathbf{x}} = [\mathbf{M}_h - \mathbf{I}](\tilde{\mathbf{x}})$, where \mathbf{I} is the identity map. In what follows, for the sake of simplicity, we will remove the subscript “ \mathbf{M}_h ” from $\mathbf{d}_{\mathbf{M}_h}$ and we will write \mathbf{d} , instead.

With the purpose of imposing boundary conditions on $\tilde{\Gamma}_h$ rather than Γ , a *shift* operator can be defined on $\tilde{\Gamma}_h$ through a Taylor expansion along \mathbf{d} , namely $\mathbf{S}_h v := v + \nabla v \cdot \mathbf{d}$. With this approach, for example, a Dirichlet boundary condition $v = g(\mathbf{x})$ on Γ is transformed into a surrogate boundary condition $\mathbf{S}_h v = g(\mathbf{M}_h(\tilde{\mathbf{x}}))$.

2.2. Shifts by way of extension operators

The Taylor expansion, however, is not the only way to construct an extension to Γ of a field v defined on the surrogate domain $\tilde{\Omega}_h$. We propose here an alternative strategy, more compatible with the typical data structures of mesh-free methods.

Assumption 1. We will assume that the grid is two-dimensional and composed of the union of triangles. With some adjustments, the following results can be extended to the case of quadrilateral grids in two dimensions and also three-dimensional grids.

We start with three definitions that will be useful in what follows.

Definition 1. Let Ω_h^f be the union of the elements between $\tilde{\Gamma}_h$ and $\hat{\Gamma}_h$, that is the union of the elements intersected by the true boundary Γ . Namely:

$$\Omega_h^f = \{T \in \mathcal{T}_h : T \cap \Gamma \neq \emptyset\}.$$

Definition 2. Let $\tilde{\Omega}_h^+ = \tilde{\Omega}_h \cup \Omega_h^f$.

Definition 3. Let $V_h(\tilde{\Omega}_h) := \{v_h \in C^0(\tilde{\Omega}_h) | v_h|_T \in \mathcal{P}^1(T), \forall T \in \tilde{\mathcal{T}}_h\}$ be the space of globally continuous functions over $\tilde{\Omega}_h$ that are piecewise linear over each $T \in \tilde{\mathcal{T}}_h$. Let the space $V_h(\tilde{\Omega}_h^+)$ be defined in an analogous way, that is, $V_h(\tilde{\Omega}_h^+) := \{v_h \in C^0(\tilde{\Omega}_h^+) | v_h|_T \in \mathcal{P}^1(T), \forall T \in \mathcal{T}_h \text{ with } T \subset \tilde{\Omega}_h^+\}$

With the previous definitions, the extension E_h can be described as the map

$$\begin{aligned} E_h : V_h(\tilde{\Omega}_h) &\rightarrow V_h(\tilde{\Omega}_h^+), \\ v_h &\mapsto E_h v_h. \end{aligned}$$

In particular, we require the consistency property that $(E_h v_h)|_{\tilde{\Omega}_h} = v_h$, for any $v_h \in V_h(\tilde{\Omega}_h)$.

3. The SBM for the Poisson equation

Let Ω be a bounded and connected open subset of \mathbb{R}^{n_d} with Lipschitz-continuous boundary $\Gamma = \partial\Omega$, which is partitioned as $\Gamma = \Gamma_D \cup \Gamma_N$ with $\Gamma_D \cap \Gamma_N = \emptyset$. Specifically, Γ_D is the Dirichlet boundary and Γ_N is the Neumann boundary. The strong form of the Poisson problem with a non-homogeneous Dirichlet and Neumann boundary condition reads

$$-\Delta u = f \quad \text{in } \Omega, \quad (4a)$$

$$u = u_D \quad \text{on } \Gamma_D, \quad (4b)$$

$$\nabla u \cdot \mathbf{n} = g_N \quad \text{on } \Gamma_N, \quad (4c)$$

where u is the solution field, u_D its value on the Dirichlet boundary Γ_D , g_N the value of the normal gradient along the Neumann boundary Γ_N , and f a source term.

3.1. Existence, uniqueness and regularity of the infinite dimensional problem

Let us denote by $H^{1/2}(\Omega)$ a fractional trace space (typically associated with $H^1(\Omega)$), and $H^{-1}(\Omega)$ the dual (space) of $H_0^1(\Omega)$. The well-posedness of the infinite dimensional problem is discussed, for example, in [50] (Theorem 5.1, p. 80), with the following result:

Theorem 1 (Well-Posedness of the Infinite-Dimensional Problem). *Let Ω be a bounded and connected open subset of \mathbb{R}^{n_d} with Lipschitz-continuous boundary $\Gamma \equiv \Gamma_D$ (pure Dirichlet problem). Given $f \in H^{-1}(\Omega)$ and $u_D \in H^{1/2}(\Gamma)$, there exists a unique solution $u \in H^1(\Omega)$ of Problem (4) with pure Dirichlet conditions. Furthermore, if the boundary Γ is of class \mathcal{C}^2 , $f \in L^2(\Omega)$ and $u_D \in H^{3/2}(\Gamma)$, then $u \in H^2(\Omega)$ and satisfies*

$$\|u\|_{2,\Omega} \leq C (\|f\|_{0,\Omega} + \|u_D\|_{3/2,\Gamma}) \quad (5)$$

for a constant C independent of f and u_D .

3.2. Weak discrete formulation

We propose the following discretization of Problem (4), inspired by Nitsche's method [51,52] for the weak enforcement of boundary conditions:

Find $u_h \in V_h(\tilde{\Omega}_h)$ such that, $\forall w_h \in V_h(\tilde{\Omega}_h)$

$$\begin{aligned} \langle \nabla u_h, \nabla w_h \rangle_{\tilde{\Omega}_h} - \langle \nabla u_h \cdot \tilde{\mathbf{n}}, w_h \rangle_{\tilde{\Gamma}_h} - \langle \mathbf{E}_h u_h - u_D, \nabla(\mathbf{E}_h w_h) \cdot \mathbf{n} - \alpha h_{\perp}^{-1} \mathbf{E}_h w_h \rangle_{\Gamma_D} \\ + \langle \mathbf{E}_h(w_h), \nabla(\mathbf{E}_h u_h) \cdot \mathbf{n} - g_N \rangle_{\Gamma_N} = \langle f, w_h \rangle_{\tilde{\Omega}_h}, \end{aligned} \quad (6)$$

where

$$h_{\perp} := \frac{\text{meas}_{n_d}(T)}{\text{meas}_{n_d-1}(\tilde{E})}, \quad (7)$$

with \tilde{E} is an edge/face of the mesh lying on $\tilde{\Gamma}_h$ such that $\tilde{E} \subset \partial T \cap \tilde{\Gamma}_h$ and $T \in \tilde{\mathcal{T}}_h$. In what follows, besides the shape-regularity of the grids, we will assume that there exist two global constants $\xi_1, \xi_2 \in \mathbb{R}^+$ such that $\xi_1 h \leq h_{\perp} \leq \xi_2 h$, so that h and h_{\perp} can be assumed interchangeable.

Remark 1. The proposed variational form bears some similarities with the work of Lozinski and co-authors [25,53]. However in [25] the domain $\tilde{\Omega}_h \supset \Omega$, the operator \mathbf{E}_h is not introduced, and appropriate ghost penalty operators are required for the stability of the discrete formulation. We prefer to introduce the operator \mathbf{E}_h and avoid ghost penalties, which require additional user-defined parameters in the variational formulation.

In the case when Neumann boundary conditions are present, in order to maintain optimal accuracy, we will also consider a mixed formulation inspired [42,46], which employs piecewise-linear, globally continuous interpolations for both the primary variable u and its gradient. Let

$$\mathbf{V}_h(\tilde{\Omega}_h) := \left\{ \mathbf{v}_h \in (C^0(\tilde{\Omega}_h))^{n_d} \mid \mathbf{v}_h|_T \in (\mathcal{P}^1(T))^{n_d}, \forall T \in \tilde{\mathcal{T}}_h \right\} \quad (8)$$

be the space of globally continuous, piecewise-linear vector functions. The mixed variational form of the SBM with extension operators reads:

Find $u_h \in V_h(\tilde{\Omega}_h)$ and $\beta_h \in \mathbf{V}_h(\tilde{\Omega}_h)$ such that, for any $w_h \in V_h(\tilde{\Omega}_h)$ and any $\psi_h \in \mathbf{V}_h(\tilde{\Omega}_h)$,

$$\begin{aligned} 0 = & \langle \beta_h, \nabla w_h \rangle_{\tilde{\Omega}_h} - \langle \beta_h \cdot \tilde{\mathbf{n}}, w_h \rangle_{\tilde{\Gamma}_h} - \langle f, w_h \rangle_{\tilde{\Omega}_h} + \langle \beta_h - \nabla u_h, \psi_h \rangle_{\tilde{\Omega}_h} \\ & - \langle \mathbf{E}_h u_h - u_D, (\mathbf{E}_h \psi_h) \cdot \mathbf{n} - \alpha h_{\perp}^{-1} \mathbf{E}_h w_h \rangle_{\Gamma_D} + \langle (\mathbf{E}_h \beta_h) \cdot \mathbf{n} - g_N, \mathbf{E}_h w_h \rangle_{\Gamma_N} \\ & + \langle \nabla \cdot \beta_h + f, \tau_u \nabla \cdot \psi_h \rangle_{\tilde{\Omega}_h} - \langle \beta_h - \nabla u_h, \tau_{\beta} (\psi_h + \nabla w_h) \rangle_{\tilde{\Omega}_h}, \end{aligned} \quad (9)$$

where β_h is a new nodal variable that approximates the gradient of u . The last two terms in (9) are appropriate variational multiscale stabilization terms that were originally introduced in [54]. In the numerical computations that follow, $\alpha = 10.0$, $\tau_u = h\bar{l}(\Omega)$, and $\tau_{\beta} = 1/2$, with $\bar{l}(\Omega)$ the largest dimension of the bounding box of Ω .

4. The SBM for the linear elasticity equations

We will also consider the equations of (compressible) linear elasticity, which are more relevant in practical applications. Their strong form is given as

$$-\nabla \cdot (\boldsymbol{\sigma}(\mathbf{u})) = \mathbf{b} \quad \text{in } \Omega, \quad (10a)$$

$$\mathbf{u} = \mathbf{u}_D \quad \text{on } \Gamma_D, \quad (10b)$$

$$\boldsymbol{\sigma} \mathbf{n} = \mathbf{t}_N \quad \text{on } \Gamma_N, \quad (10c)$$

where \mathbf{u} is the displacement field, \mathbf{u}_D its value on the Dirichlet boundary Γ_D , \mathbf{t}_N the traction along the Neumann boundary Γ_N , and \mathbf{b} a body force. The stress $\boldsymbol{\sigma}$ is a linear function of \mathbf{u} , according to the constitutive model

$$\boldsymbol{\sigma}(\mathbf{u}) = \mathbf{C}\boldsymbol{\varepsilon}(\mathbf{u}),$$

where \mathbf{C} is the fourth-order elasticity tensor. Recalling the definition (8), we will then consider the following variational formulation, which can be considered a vectorial generalization of (6):

Find $\mathbf{u}_h \in \mathbf{V}_h(\tilde{\Omega}_h)$ such that, $\forall \mathbf{w}_h \in \mathbf{V}_h(\tilde{\Omega}_h)$,

$$\begin{aligned} & \langle \mathbf{C}\boldsymbol{\varepsilon}(\mathbf{u}_h), \boldsymbol{\varepsilon}(\mathbf{w}_h) \rangle_{\tilde{\Omega}_h} - \langle \mathbf{C}\boldsymbol{\varepsilon}(\mathbf{u}_h), \mathbf{w}_h \otimes \tilde{\mathbf{n}} \rangle_{\tilde{\Gamma}_h} - \langle (\mathbf{E}_h \mathbf{u}_h - \mathbf{u}_D) \otimes \mathbf{n}, \mathbf{C}\boldsymbol{\varepsilon}(\mathbf{E}_h \mathbf{w}_h) \rangle_{\Gamma_D} + \langle \mathbf{E}_h \mathbf{u}_h - \mathbf{u}_D, \alpha |\mathbf{C}| h_{\perp}^{-1} \mathbf{E}_h \mathbf{w}_h \rangle_{\Gamma_D} \\ & + \langle \mathbf{E}_h \mathbf{w}_h, (\mathbf{C}\boldsymbol{\varepsilon}(\mathbf{u}_h)) \cdot \mathbf{n} - \mathbf{t}_N \rangle_{\Gamma_N} = \langle \mathbf{b}, \mathbf{w}_h \rangle_{\tilde{\Omega}_h}, \end{aligned} \quad (11)$$

where $|\mathbf{C}|$ is the Frobenius norm of the tensor \mathbf{C} .

Remark 2. Observe that in the case in which $\tilde{\Omega}_h \equiv \Omega$, that is $\tilde{\Gamma}_h \equiv \Gamma$ and $\mathbf{E}_h \equiv \mathbf{I}$, (11) collapses to the canonical Nitsche's variational formulation:

$$\begin{aligned} & \langle \mathbf{C}\boldsymbol{\varepsilon}(\mathbf{u}_h), \boldsymbol{\varepsilon}(\mathbf{w}_h) \rangle_{\tilde{\Omega}_h} - \langle \mathbf{C}\boldsymbol{\varepsilon}(\mathbf{u}_h), \mathbf{w}_h \otimes \mathbf{n} \rangle_{\Gamma_D} - \langle (\mathbf{u}_h - \mathbf{u}_D) \otimes \mathbf{n}, \mathbf{C}\boldsymbol{\varepsilon}(\mathbf{w}_h) \rangle_{\Gamma_D} \\ & + \langle \mathbf{u}_h - \mathbf{u}_D, \alpha |\mathbf{C}| h_{\perp}^{-1} \mathbf{w}_h \rangle_{\Gamma_D} - \langle \mathbf{w}_h, \mathbf{t}_N \rangle_{\Gamma_N} = \langle \mathbf{b}, \mathbf{w}_h \rangle_{\tilde{\Omega}_h}. \end{aligned} \quad (12)$$

5. Extension operators

We will consider two different definitions of \mathbf{E}_h . Consider the following definition of the extension operator:

$$\mathbf{E}_h v_h(\mathbf{x}) := \sum_{A \in \tilde{\mathcal{N}}} N_A(\mathbf{x}) \mathbf{v}_A + \sum_{B \in \hat{\mathcal{N}}} N_B(\mathbf{x}) \hat{\mathbf{v}}_B, \quad (13)$$

where $\tilde{\mathcal{N}}$ is the set of nodes (vertices) of the grid that belong to $\tilde{\Omega}_h$, $\hat{\mathcal{N}}$ is the set of nodes of the grid on $\hat{\Gamma}_h$, and N_A and N_B are the finite element shape functions associated with nodes $A \in \tilde{\mathcal{N}}$ and $B \in \hat{\mathcal{N}}$, respectively. $\mathbf{v}_A = v_h(\mathbf{x}_A)$ represent the nodal values of v_h over $\tilde{\Omega}_h$ and the extension operator \mathbf{E}_h is defined by the nodal values $\hat{\mathbf{v}}_B$ over $\hat{\Gamma}_h$. Similarly the gradient of the extension $\mathbf{E}_h v_h$ of v_h is computed as:

$$\nabla(\mathbf{E}_h v_h)(\mathbf{x}) := \sum_{A \in \tilde{\mathcal{N}}} \nabla N_A(\mathbf{x}) \mathbf{v}_A + \sum_{B \in \hat{\mathcal{N}}} \nabla N_B(\mathbf{x}) \hat{\mathbf{v}}_B, \quad (14)$$

Next, we consider two different extension operators.

5.1. An extension operator based on the average gradient

This first strategy for the construction of the extension operator relies on computing a discrete gradient $\tilde{\mathbf{G}}(\cdot) = \{\tilde{\mathbf{G}}_d(\cdot)\}_{d=1}^{n_d}$ on nodes located along the boundary $\tilde{\Gamma}_h$ by way of the (lumped) L^2 -projection of gradients from neighboring elements. We will describe this approach for simplex-type elements (for which elemental gradients are constant), but similar derivations apply to quadrilateral or hexahedral elements.

Let $\tilde{\mathcal{T}}_{h:A} := \{T \in \tilde{\mathcal{T}}_h : T \cap A \neq \emptyset\}$ be the set of elements in $\tilde{\Omega}_h$ that share node A , and \mathcal{N}_T the set of nodes that belong to element T . Then we define

$$(\tilde{\mathbf{G}}v_h)_A = \frac{1}{\sum_{T \in \tilde{\mathcal{T}}_{h:A}} |T|} \sum_{T \in \tilde{\mathcal{T}}_{h:A}} |T| \nabla v_h|_T = \frac{1}{\sum_{T \in \tilde{\mathcal{T}}_{h:A}} |T|} \sum_{T \in \tilde{\mathcal{T}}_{h:A}} |T| \sum_{B \in \mathcal{N}_T} (\nabla N_B)|_T \mathbf{v}_B, \quad (15)$$

where $|T| = \text{meas}_{n_d}(T)$ is the measure of the element T (area/volume in two/three dimensions). In plain words, we associate to each node the area/volume-weighted average of the gradients of the elements that share it as shown in Fig. 2. More specifically, Figs. 2(a), 2(b), and 2(c) show which elements inside $\tilde{\Omega}_h$ are involved in the calculation of the nodal gradient $\tilde{\mathbf{G}}$ associated with three different nodes on $\tilde{\Gamma}_h$.

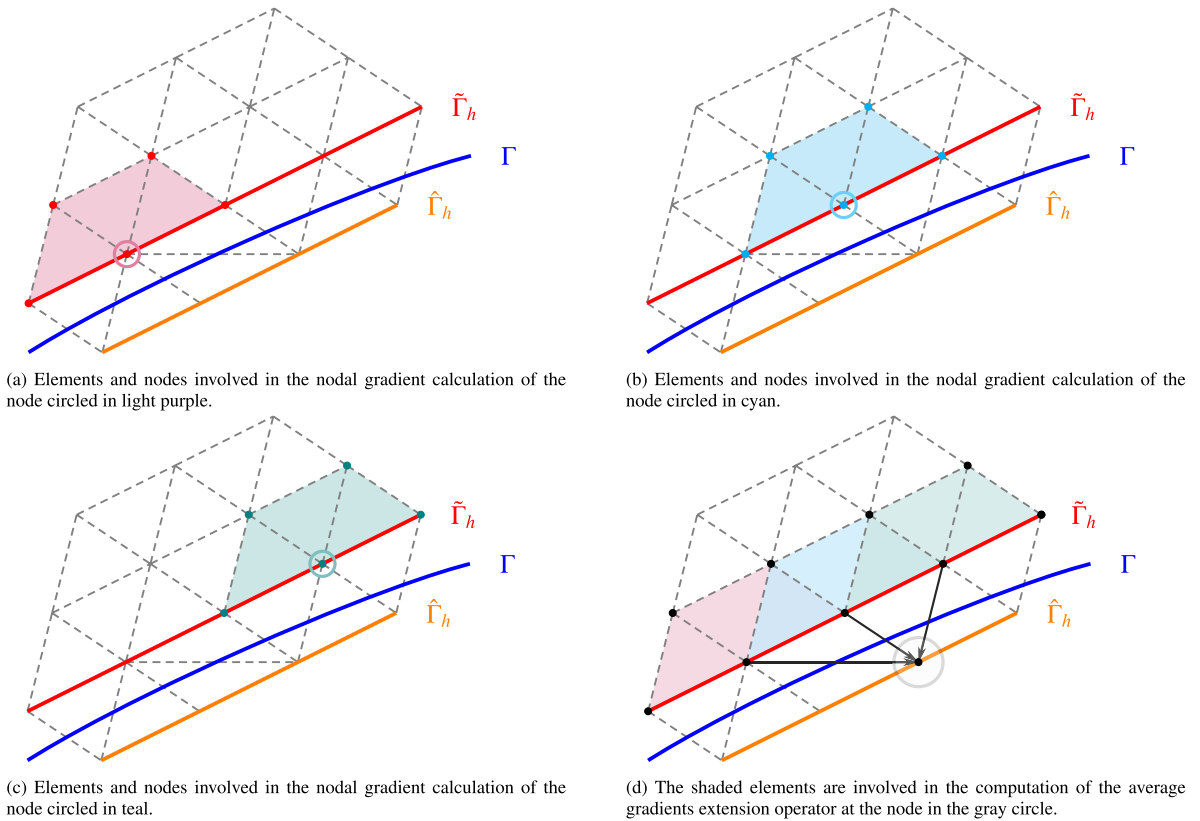


Fig. 2. Extension by average gradients. The blue, red and orange curves represent the true boundary Γ and surrogate boundaries $\tilde{\Gamma}_h$ and $\hat{\Gamma}_h$, respectively. (For interpretation of the references to color in this figure legend, the reader is referred to the web version of this article.)

The extension of v_h to a node B on $\hat{\Gamma}_h$ is then constructed as the weighted average of the linear extrapolations of v_h along each edge e_{AB} connecting A to B , where each weight is the inverse of the edge length $|e_{AB}| = |\mathbf{x}_B - \mathbf{x}_A|$. Namely:

$$\hat{v}_B := E_h v_h(\mathbf{x}_B) = \frac{1}{\sum_{A \in \tilde{\mathcal{N}}_B} |e_{AB}|^{-1}} \sum_{A \in \tilde{\mathcal{N}}_B} |e_{AB}|^{-1} (v_A + (\tilde{\mathbf{G}}v_h)_A \cdot e_{AB}), \quad (16)$$

where $\tilde{\mathcal{N}}_B$ is the set of nodes on $\tilde{\Gamma}_h$ that are connected by an edge e_{AB} to node B and we used \hat{v}_B as the short-hand notation for $E_h v_h(\mathbf{x}_B)$, with $B \in \hat{\mathcal{N}}$. Fig. 2(d) depicts the final stage of the extension procedure, and all the elements and nodes involved in the calculation of (16). For simplicity, we will rewrite (16) as

$$E_h v_h(\mathbf{x}_B) = \sum_{A \in \tilde{\mathcal{N}}_B} \alpha_{BA} (v_A + (\tilde{\mathbf{G}}v_h)_A \cdot e_{AB}), \quad \text{with} \quad \alpha_{BA} = \frac{|e_{AB}|^{-1}}{\sum_{A \in \tilde{\mathcal{N}}_B} |e_{AB}|^{-1}}. \quad (17)$$

Remark 3. It is easily seen that $\sum_{A \in \tilde{\mathcal{N}}_B} \alpha_{BA} = 1$ and that $(E_h v_h)|_{\hat{\Omega}_h} = v_h$, for any $v_h \in V_h(\hat{\Omega}_h)$.

Similarly, (15) can be refactored as

$$(\tilde{\mathbf{G}}v_h)_A = \sum_{T \in \tilde{\mathcal{T}}_{h:A}} \beta_{A,T} \nabla v_h|_T, \quad \text{with} \quad \beta_{A,T} = \frac{|T|}{\sum_{T \in \tilde{\mathcal{T}}_{h:A}} |T|} \quad (18)$$

and $\sum_{T \in \tilde{\mathcal{T}}_{h:A}} \beta_{A,T} = 1$.

5.2. An extension operator based on moving least-squares

A second extension operator we consider stems from meshfree numerical methods, such as the Diffuse Element Method [55], and leverages a Moving Least-Squares (MLS) approximation of the field of interest.

We start by defining the cloud of sample nodes over which the least-square procedure will be used. Given a node $B \in \hat{\mathcal{N}}$, we consider the set $\tilde{\mathcal{N}}_B$ of nodes that are connected to B by a single edge, that is the first ‘‘layer’’ of neighboring nodes, shown in

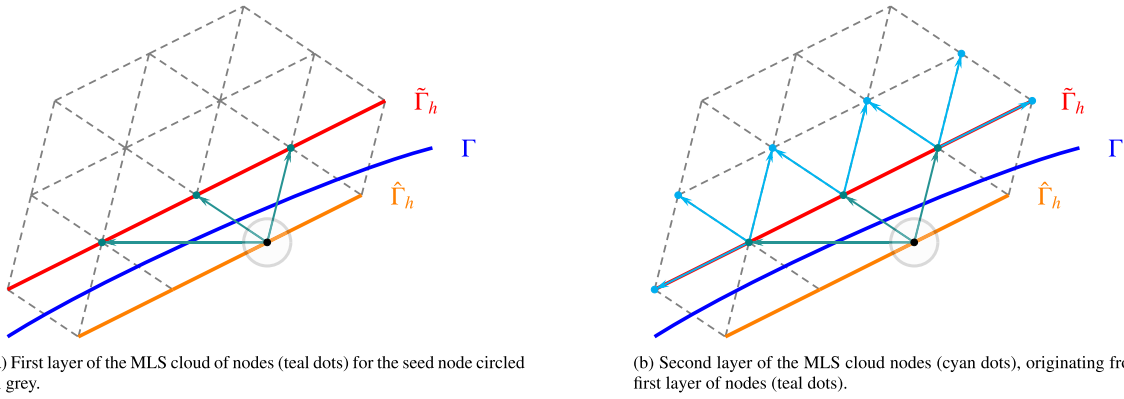


Fig. 3. Extension by MLS. The blue, red and orange curves represent the true boundary Γ and surrogate boundaries $\tilde{\Gamma}_h$ and $\hat{\Gamma}_h$, respectively. For a seed node on $\hat{\Gamma}_h$, circled in grey, the figure shows the cloud of sample nodes utilized by the MLS extension operator. (For interpretation of the references to color in this figure legend, the reader is referred to the web version of this article.)

Fig. 3(a). The second layer in the cloud is the set of nodes in $\tilde{\Omega}_h$ that are edge-neighbors of nodes in the first layer, as shown in **Fig. 3(b)**, and so forth. Note that the first layer of nodes lies on $\tilde{\Gamma}_h$, but all other layers may include also nodes that lie on the interior of $\tilde{\Omega}_h$.

In order to obtain a well-posed (non-singular) MLS algebraic problem, the sample nodes must be in sufficient number and distributed with some uniformity. These two requirements are normally met by immersed grids, which maintain good quality metrics as they do not need to conform to the geometry of boundaries. In addition, depending on the order of the polynomial used in the MLS approximation, there is a minimal requirement on the number of layers to be used: for first-order (linear) approximation, at least two layers are required; for second-order accuracy, at least three layers are required; etc. In all numerical tests, we will always choose the minimal number of layers necessary to achieve the accuracy of the interpolation utilized.

Let \mathcal{N}_B^{MLS} be the chosen cloud of sample nodes associated with $B \in \hat{\mathcal{N}}$. The MLS approximation takes the form

$$\hat{v}_B = \sum_{A \in \mathcal{N}_B^{MLS}} \omega_{BA} v_A, \tag{19}$$

where the ω_{BA} 's are appropriate weights that must fulfill the partition of unity property $\sum_{A \in \mathcal{N}_B^{MLS}} \omega_{BA} = 1$. These weights are obtained by solving an appropriate least-square minimization problem, which we describe next in the case of first-order approximation. The procedure for higher-order approximations will be very similar. A linear approximation to $v_h(\mathbf{x})$ in a neighborhood of the node B (of coordinate \mathbf{x}_B) can be cast in the form

$$v_h(\mathbf{x}) \approx \mathbf{c}[B]^T \mathbf{p}(\mathbf{x}), \tag{20}$$

where

$$\mathbf{p}(\mathbf{x}) = [1, x, y]^T$$

in two dimensions, and

$$\mathbf{p}(\mathbf{x}) = [1, x, y, z]^T$$

in three dimensions. Here the notation $\mathbf{c}[B]$ indicates that the array of coefficients \mathbf{c} depends on the seed node B . $\mathbf{c}[B]$ is obtained as the solution to the least-squares minimization problem

$$\arg \min_{\mathbf{c}[B] \in \mathbb{R}^{n_d+1}} \sum_{A \in \mathcal{N}_B^{MLS}} \phi(\mathbf{x}_A, \mathbf{x}_B) (\mathbf{c}[B]^T \mathbf{p}(\mathbf{x}_A) - v_A)^2, \tag{21}$$

where we have introduced the Gaussian smoothing kernel

$$\phi(\mathbf{x}_A, \mathbf{x}_B) = \exp\left(-\frac{|e_{AB}|}{2(\max_{A \in \mathcal{N}_B^{MLS}} |e_{AB}|)^2}\right),$$

which adds more weight to the information near node B . Again, $|e_{AB}| = |\mathbf{x}_B - \mathbf{x}_A|$ denotes the length of the segment e_{AB} connecting node A and node B . The classic closed form of the minimization problem (21) is given by

$$\mathbf{c}[B] = \mathbf{M}[B]^{-1} \sum_{A \in \mathcal{N}_B^{MLS}} \phi(\mathbf{x}_A, \mathbf{x}_B) \mathbf{p}(\mathbf{x}_A) v_A, \tag{22}$$

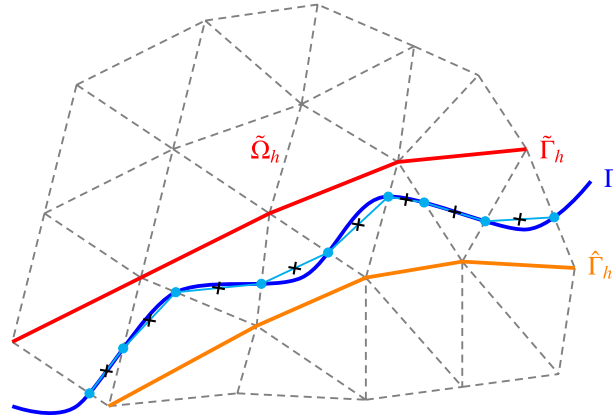


Fig. 4. Integration over Γ (in blue). The intersections of Γ with the underlying grid (light blue dots), the piecewise-linear interpolate Γ_h of Γ (light blue segments), and the quadrature points associated with the mid-point quadrature integration rule (black crosses). (For interpretation of the references to color in this figure legend, the reader is referred to the web version of this article.)

where $\mathbf{M}[B]$ the Gramian matrix

$$\mathbf{M}[B] = \sum_{A \in \mathcal{N}_B^{MLS}} \phi(\mathbf{x}_A, \mathbf{x}_B) \mathbf{p}(\mathbf{x}_A) \mathbf{p}^T(\mathbf{x}_A).$$

Substituting (22) into (20) yields

$$\hat{\mathbf{v}}_B \approx \mathbf{p}^T(\mathbf{x}_B) \mathbf{M}[B]^{-1} \left(\sum_{A \in \mathcal{N}_B^{MLS}} \phi(\mathbf{x}_A, \mathbf{x}_B) \mathbf{p}(\mathbf{x}_A) \mathbf{v}_A \right),$$

which is equivalent to setting

$$\omega_{BA} = \phi(\mathbf{x}_A, \mathbf{x}_B) \mathbf{p}^T(\mathbf{x}_B) \mathbf{M}[B]^{-1} \mathbf{p}(\mathbf{x}_A)$$

in (19).

Remark 4. The partition of unity property

$$\sum_{A \in \mathcal{N}_B^{MLS}} \omega_{BA} = 1 \tag{23}$$

can be easily proved starting from (19) and using the property that the least-square extrapolation is exact up to linear fields by construction. Hence considering the constant field $v_h = 1$ and substituting $\hat{\mathbf{v}}_B = 1$ and $\mathbf{v}_A = 1$ in (19), we obtain (23).

Remark 5. Each coefficient ω_{BA} only depends on the mesh and can be computed once and for all in a pre-processing stage of the computations.

5.3. Integration of the variational terms involving the extension operators

One key aspect that has not yet been discussed is the integration of the variational terms defined over the boundary Γ and involving the extension operator. This procedure requires the definition of specific integration points along Γ and corresponding weights. We will describe it only in the two-dimensional case for triangular elements. The discussion can be generalized to quadrilateral elements in two dimensions and tetrahedral or hexahedral elements in three dimensions.

Given a geometric representation of Γ (e.g., a level-set, an STL surface, etc.), the integration procedure can be devised in multiple stages (see Fig. 4 for reference):

1. Construct the extension operators over the cloud of points $\hat{\mathcal{N}}$.
2. Compute the intersections of the true boundary with the underlying immersed grid (the light blue dots in Fig. 4), and approximate the true boundary Γ with a piecewise-linear polygonal curve Γ_h (the light blue segmented curve in Fig. 4), connecting the intersection points with straight segments.
3. Define a quadrature formula on each of the segments composing Γ_h (e.g., the mid-point formula, depicted with black crosses in Fig. 4).

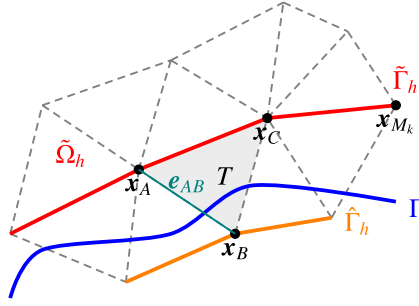


Fig. 5. Auxiliary sketch for the proof of Lemma 2.

The proposed interpolation and integration approach is second-order accurate, and therefore compatible with the order of approximation of the proposed SBM. Of course, one could use more general representations of the surface than just a polygonal curve, and, analogously, one could use integration rules more general than the simple mid-point rule.

5.4. Properties of the extension operator E_h

This section is devoted to the derivation of the main abstract properties of the extension operator E_h introduced in Section 2.2. This is a very technical section and the reader could simply browse through it in a first reading of the article. The main results are summarized in a number of lemmas and corollaries that will be used in the numerical analysis described in Section 6.

In what follows, the notation $a \lesssim b$, for some quantities a and b that depend on the triangulation \mathcal{T}^h , indicates that $a \leq cb$, for some positive real constant c independent of \mathcal{T}^h . The first important result is the following fundamental lemma:

Lemma 1. *Let T be a triangular element contained in Ω_h^Γ and let $\mathcal{T}_{\mathcal{N}}^h(T)$ be the set of triangles in $\tilde{\Omega}_h$ whose vertices influence the definition of the extension operator E_h on the triangle T . Then it holds:*

$$\|\nabla E_h v_h\|_{0,T} \lesssim \|\nabla v_h\|_{0,\mathcal{T}_{\mathcal{N}}^h(T)}, \quad \forall v_h \in V_h(\tilde{\Omega}_h).$$

Proof. The proof of Lemma 1 is based on the following technical lemma:

Lemma 2. *Given any triangle T with vertices x_A , x_B , and x_C then*

$$\int_T \|\nabla v_h\|^2 dx \simeq |v_h(x_A) - v_h(x_C)|^2 + |v_h(x_B) - v_h(x_C)|^2, \quad \forall v_h \in \mathcal{P}^1(T),$$

where the symbol “ \simeq ” indicates equivalency up to a positive constant.

Proof. Both sides are invariant under affine transformations, so it is enough to map back to the parent (reference) element \hat{T} and use the equivalence of the norms in $\mathcal{P}^1(T)/\mathbb{R}$. \square

We will now proceed with the proof of Lemma 1, distinguishing between the case of the gradient-based and the moving least-squares extension operator.

Gradient-based extension. Consider the situation depicted in Fig. 5. Recalling (17) and (18), and using Remark 3, we have:

$$\hat{v}_B - v_C = \sum_{A \in \tilde{\mathcal{N}}_B} \alpha_{BA} (v_A - v_C - (\hat{\mathbf{G}}v_h)_A \cdot e_{AB}) = \sum_{A \in \tilde{\mathcal{N}}_B, A \neq C} \alpha_{BA} (v_A - v_C) - \sum_{A \in \tilde{\mathcal{N}}_B} \alpha_{BA} (\hat{\mathbf{G}}v_h)_A \cdot e_{AB}.$$

Now, if the nodes A and C belong to the same triangle T , then $v_A - v_C = \nabla v_h|_T \cdot e_{AC}$ and

$$|v_A - v_C|^2 \leq \|\nabla v_h|_T\|^2 \|e_{AC}\|^2 \lesssim h_T^2 |\nabla v_h|_T|^2 \simeq \int_T |\nabla v_h|^2. \tag{24}$$

Instead, if node A and C do not belong to the same triangle, but are connected by p triangles, one has

$$v_A - v_C = (v_A - v_{M_1}) + (v_{M_1} - v_{M_2}) + (v_{M_2} - v_{M_3}) + \dots + (v_{M_{p-1}} - v_C)$$

and the previous estimate can be applied term by term. Thus,

$$\left(\sum_{A \in \tilde{\mathcal{N}}_B} \alpha_{BA} (v_A - v_C) \right)^2 \leq \underbrace{\sum_{A \in \tilde{\mathcal{N}}_B} \alpha_{BA}^2}_{\leq 1} \sum_{A \in \tilde{\mathcal{N}}_B} (v_A - v_C)^2 \leq \sum_{T' \in \mathcal{T}_{AC}^h(\tilde{\Omega}_h)} \int_{T'} |\nabla v_h|^2$$

for a set of triangles $\mathcal{T}'_{AC}(\tilde{\Omega}_h)$ connecting node A and C . On the other hand,

$$\left| (\tilde{\mathbf{G}}v_h)_A \cdot e_{AB} \right|^2 = \left| \sum_{T \in \mathcal{T}'_{h:A}} \beta_{A,T} \nabla v_h|_T \cdot e_{AB} \right|^2 \leq \underbrace{\sum_{T \in \mathcal{T}'_{h:A}} \beta_{A,T}^2}_{\leq 1} \sum_{T \in \mathcal{T}'_{h:A}} \|\nabla v_h|_T\|^2 \underbrace{\|e_{AB}\|^2}_{\approx \|e_{AC}\|^2} \lesssim \sum_{T \in \mathcal{T}'_{h:A}} \int_T |\nabla v_h|^2, \tag{25}$$

so that

$$\left(\sum_{A \in \tilde{\mathcal{N}}_B} (\tilde{\mathbf{G}}v_h)_A \cdot e_{AB} \right)^2 \leq \underbrace{\text{card}(\tilde{\mathcal{N}}_B)}_{O(1)} \sum_{A \in \tilde{\mathcal{N}}_B} \left((\tilde{\mathbf{G}}v_h)_A \cdot e_{AB} \right)^2 \lesssim \sum_{A \in \tilde{\mathcal{N}}_B} \sum_{T \in \mathcal{T}'_{h:A}} \int_T |\nabla v_h|^2.$$

Moving least-square extension. In this case, recalling (19) and Remark 4, we have

$$\hat{v}_B - v_C = \sum_{A \in \mathcal{N}_B^{MLS}} \omega_{BA} (v_A - v_C),$$

and arguments similar to the case of the gradient-based extension operator can be used. \square

We consider next a number of important results that are consequences of Lemma 1.

Corollary 1. *It holds*

$$h_T^{1/2} \|\nabla E_h v_h\|_{0,T \cap \Gamma} \lesssim \|\nabla v_h\|_{0,\mathcal{T}'_h(T)}, \quad \forall v_h \in V_h(\tilde{\Omega}_h).$$

Proof. We have

$$h_T \|\nabla E_h v_h\|_{0,T \cap \Gamma}^2 = \underbrace{|\langle \nabla E_h v_h \rangle|_T|^2}_{\text{constant}} h_T \int_{0,T \cap \Gamma} d\Gamma \lesssim |\langle \nabla E_h v_h \rangle|_T|^2 \int_T d\tilde{\Omega}_h = \|\nabla E_h v_h\|_{0,T}^2. \quad \square$$

Corollary 2. *There exists a constant c_* , independent of the mesh size, such that*

$$\|h^{1/2} \nabla(E_h v_h)\|_{0,\Gamma} \leq c_* \|\nabla v_h\|_{0,\tilde{\Omega}_h}, \quad \forall v_h \in V_h(\tilde{\Omega}_h).$$

Proof. This result easily follows from the scaled trace inequality (Theorem 5), together with Lemma 1. The constant c_* is independent from the mesh size, as it depends on the constants appearing in the statements of Theorem 5 and Lemma 1 \square

Corollary 3. *There exists a constant c_{\circledast} , independent of the mesh size, such that*

$$\|v_h\|_{0,\tilde{\Gamma}_h} \leq c_{\circledast} \left(\|E_h v_h\|_{0,\Gamma} + \max_{\tilde{\Gamma}_h} |\mathbf{d}| \|\nabla v_h\|_{0,\tilde{\Omega}_h} \right), \quad \forall v_h \in V_h(\tilde{\Omega}_h).$$

Proof. Observe that, by definition, $(E_h v_h)|_{\tilde{\Gamma}_h} = v_h|_{\tilde{\Gamma}_h}$ and, looking at the sketch of Fig. 6, notice that the following identity holds:

$$E_h v_h(\mathbf{x}) - E_h v_h(\tilde{\mathbf{x}}) = E_h v_h(\mathbf{M}_h \tilde{\mathbf{x}}) - E_h v_h(\tilde{\mathbf{x}}) = \sum_{T' \in \mathcal{T}'(\tilde{\mathbf{x}}, \mathbf{d})} (\nabla(E_h v_h))|_{T'} \cdot \mathbf{d}_{T'},$$

where $\mathcal{T}'(\tilde{\mathbf{x}}, \mathbf{d})$ is the set of all elements of the grid that are intersected by the distance vector \mathbf{d} that maps $\tilde{\mathbf{x}}$ to \mathbf{x} and $\mathbf{d}_{T'}$ are vectors that subdivide \mathbf{d} , that is $\mathbf{d} = \sum_{T' \in \mathcal{T}'(\tilde{\mathbf{x}}, \mathbf{d})} \mathbf{d}_{T'}$ with $\mathbf{d}_{T'}$ connecting the two edges of element T' . Hence $\mathbf{d}_{T'} = \eta_{T'} \mathbf{d}$ with $\sum_{T' \in \mathcal{T}'(\tilde{\mathbf{x}}, \mathbf{d})} \eta_{T'} = 1$. Note that the cardinality of $\mathcal{T}'(\tilde{\mathbf{x}}, \mathbf{d})$ is finite since the mesh must be regular and therefore the angles formed by the corners of the elements must be uniformly bounded from below. The graphical sketch of Fig. 6 refers to the case in which $\text{card}(\mathcal{T}'(\tilde{\mathbf{x}}, \mathbf{d})) = 2$. Whence,

$$|E_h v_h(\tilde{\mathbf{x}})|^2 \lesssim |E_h v_h(\mathbf{M}_h \tilde{\mathbf{x}})|^2 + \sum_{T' \in \mathcal{T}'(\tilde{\mathbf{x}}, \mathbf{d})} |\eta_{T'}|^2 |\langle \nabla(E_h v_h) \rangle|_{T'}|^2 |\mathbf{d}|^2.$$

Integrating over $T \cap \tilde{\Gamma}_h$ (recall that $T \cap \tilde{\Gamma}_h$ may be just a vertex of T) for an element $T \in \Omega_h^f$ yields

$$\|v_h\|_{0,T \cap \tilde{\Gamma}_h}^2 \lesssim \|E_h v_h\|_{0,T \cap \tilde{\Gamma}_h}^2 + \left(\sum_{T' \in \mathcal{T}'(\tilde{\mathbf{x}}, \mathbf{d})} |\langle \nabla(E_h v_h) \rangle|_{T'}|^2 \right) \max_{T \cap \tilde{\Gamma}_h} |\mathbf{d}|^2 \int_{T \cap \tilde{\Gamma}_h} d\tilde{\Gamma}_h \lesssim \|E_h v_h\|_{0,T \cap \tilde{\Gamma}_h}^2 + \max_{T \cap \tilde{\Gamma}_h} |\mathbf{d}|^2 \|\nabla E_h v_h|_T\|_{0,T}^2.$$

We conclude by summing over all $T \in \Omega_h^f$. \square

Remark 6. From the inspection of the proof of Corollary 3, we actually have proven the following result:

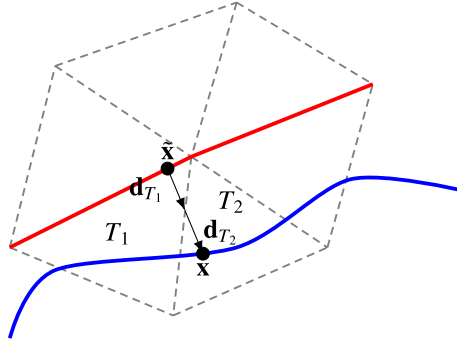


Fig. 6. Auxiliary sketch for the proof of Corollary 3.

Corollary 4. *There exists a constant \hat{c}_\otimes , independent of the mesh size, such that*

$$\|h^{-1/2}v_h\|_{0,\tilde{\Gamma}_h}^2 \leq \hat{c}_\otimes \left(\|h^{-1/2}E_h v_h\|_{0,\Gamma}^2 + \max_{T \in \Omega_h^T} \left(\frac{\max_{T \cap \tilde{\Gamma}_h} |d|}{h_T} \right) \|\nabla v_h\|_{0,\tilde{\Omega}_h}^2 \right), \quad \forall v_h \in V_h(\tilde{\Omega}_h).$$

5.4.1. The extension operator E_h in $H^2(\tilde{\Omega}_h)$

The purpose of this section is to extend some of the results of the previous section to the case in which a function is in $H^2(\tilde{\Omega}_h)$ instead of $V^h(\tilde{\Omega}_h)$. These results will be instrumental to prove convergence of the proposed algorithms in Section 6.2.

Consider now the space $V(\tilde{\Omega}_h; \tilde{\mathcal{T}}_h) = V_h(\tilde{\Omega}_h) + H^2(\tilde{\Omega}_h) \subset H^2(\tilde{\Omega}_h; \tilde{\mathcal{T}}_h)$, which extends $V_h(\tilde{\Omega}_h)$ to function spaces that can represent the exact solution of the infinite dimensional variational problem associated to (4). Consider also $H^2(\tilde{\Omega}_h; \tilde{\mathcal{T}}_h) = \prod_{T \in \tilde{\mathcal{T}}_h} H^2(T)$ with ‘broken’ norm $\|\cdot\|_{2,\tilde{\Omega}_h;\tilde{\mathcal{T}}_h} = \sum_{T \in \tilde{\mathcal{T}}_h} \|\cdot\|_{2,T}$. We associate to $V(\tilde{\Omega}_h; \tilde{\mathcal{T}}_h)$ the norm

$$\|v\|_{V(\tilde{\Omega}_h;\tilde{\mathcal{T}}_h)}^2 = \|v\|_a^2 + |hw|_{2,\tilde{\Omega}_h;\tilde{\mathcal{T}}_h}^2, \tag{26}$$

where

$$\|u_h\|_a^2 = \|\nabla u_h\|_{0,\tilde{\Omega}_h}^2 + \|h^{-1/2}E_h u_h\|_{0,\Gamma}^2, \tag{27}$$

and we note that if $v \in V_h(\tilde{\Omega}_h)$, then $\|v\|_{V(\tilde{\Omega}_h;\tilde{\mathcal{T}}_h)} = \|v\|_a$.

Definition 4. For any $w \in V(\tilde{\Omega}_h; \tilde{\mathcal{T}}_h)$, let $E_h w := E_h(l_h w)$, where $l_h w$ is the piecewise-linear function that interpolates w at the nodes of $\mathcal{T}^h(\tilde{\Omega}_h)$.

The previous definition is consistent, since if $w = w_h \in V^h(\tilde{\Omega}_h)$, then $l_h w = w_h$. Then E_h is well-defined on $V(\tilde{\Omega}_h; \tilde{\mathcal{T}}_h)$ and Corollary 2 can be extended as follows:

Corollary 5. *It holds*

$$\|h^{1/2}\nabla(E_h w)\|_{0,\Gamma} \lesssim \|w\|_{V(\tilde{\Omega}_h;\tilde{\mathcal{T}}_h)}, \quad \forall w \in V(\tilde{\Omega}_h; \tilde{\mathcal{T}}_h).$$

Proof. Applying Corollary 2, we have that

$$\begin{aligned} \|h^{1/2}\nabla(E_h w)\|_{0,\Gamma} &= \|h^{1/2}\nabla(E_h(l_h w))\|_{0,\Gamma} \lesssim \|\nabla(l_h w)\|_{0,\tilde{\Omega}_h} \\ &\leq \|\nabla w\|_{0,\tilde{\Omega}_h} + \|\nabla(w - l_h w)\|_{0,\tilde{\Omega}_h} \lesssim \|\nabla w\|_{0,\tilde{\Omega}_h} + \left(\sum_{T \in \tilde{\mathcal{T}}_h} h_T^2 |w|_{2,T} \right)^{1/2} \lesssim \|w\|_{V(\tilde{\Omega}_h;\tilde{\mathcal{T}}_h)} \quad \square \end{aligned}$$

Similarly, Corollary 4 can be extended as

Corollary 6. *For any $w \in V(\tilde{\Omega}_h; \tilde{\mathcal{T}}_h)$ it holds*

$$\|h^{-1/2}w\|_{0,\tilde{\Gamma}_h}^2 \lesssim \|h^{-1/2}E_h w\|_{0,\Gamma}^2 + \left(1 + \max_{T \in \Omega_h^T} \left(\frac{\max_{T \cap \tilde{\Gamma}_h} |d|}{h_T} \right) \right) \|w\|_{V(\tilde{\Omega}_h;\tilde{\mathcal{T}}_h)}^2.$$

Proof. We start by writing

$$\|h^{-1/2}w\|_{0,\tilde{\Gamma}_h} \leq \|h^{-1/2}l_h w\|_{0,\tilde{\Gamma}_h} + \|h^{-1/2}(w - l_h w)\|_{0,\tilde{\Gamma}_h}.$$

Observing that on \tilde{T}_h one has $l_h w = E_h(l_h w) = E_h w$, then

$$\begin{aligned} \|h^{-1/2} l_h w\|_{0,\tilde{T}_h} &= \|h^{-1/2} E_h(l_h w)\|_{0,\tilde{T}_h} \lesssim \|h^{-1/2} E_h(l_h w)\|_{0,T} + \max_{T \in \Omega_h^T} \left(\frac{\max_{T \cap \tilde{T}_h} |d|}{h_T} \right)^{1/2} \|\nabla(l_h w)\|_{0,\tilde{\Omega}_h} \\ &\lesssim \|h^{-1/2} E_h w\|_{0,T} + \max_{T \in \Omega_h^T} \left(\frac{\max_{T \cap \tilde{T}_h} |d|}{h_T} \right)^{1/2} \|w\|_{V(\tilde{\Omega}_h; \tilde{\mathcal{T}}_h)}, \end{aligned}$$

as in the proof of Corollary 5. On the other hand,

$$\begin{aligned} \|h^{-1/2}(w - l_h w)\|_{0,\tilde{T}_h}^2 &= \sum_{T \in \tilde{\mathcal{T}}^h, T \cap \tilde{T}_h \neq \emptyset} h_T^{-2} \|h^{1/2}(w - l_h w)\|_{0,T \cap \tilde{T}_h}^2 \lesssim \sum_{T \in \tilde{\mathcal{T}}^h} h_T^{-2} \left(\|w - l_h w\|_{0,T}^2 + h_T^2 \|\nabla(w - l_h w)\|_{0,T}^2 \right) \\ &\lesssim \sum_{T \in \tilde{\mathcal{T}}^h} h_T^{-2} \left(h_T^4 |w|_{2,T}^2 + h_T^4 |w|_{2,T}^2 \right) \lesssim \sum_{T \in \tilde{\mathcal{T}}^h} h_T^2 |w|_{2,T}^2 \lesssim \|w\|_{V(\tilde{\Omega}_h; \tilde{\mathcal{T}}_h)}^2, \end{aligned}$$

which concludes the proof. \square

5.4.2. Estimate of the approximation error

We wish to estimate

$$\|h^{1/2}(E_h w - w)\|_{0,T}, \quad \forall w \in H^2(\Omega). \tag{28}$$

To this end, we prove some technical lemmas:

Lemma 3. Let T be a triangle in Ω_h^T . Then $\forall z_h \in V_h(\tilde{\Omega}_h)$,

$$\|E_h z_h - z_h\|_{0,T} \simeq h_T \left(\sum_{A \in \mathcal{N}_T} |\tilde{z}_A - z_A|^2 \right)^{1/2},$$

where $z_A = z_h(\mathbf{x}_A)$, $\tilde{z}_A = (E_h z_h)(\mathbf{x}_A)$, and \mathcal{N}_T the set of nodes that belong to element T .

Proof. A scaling argument and the equivalence of norms on the reference element \hat{T} yields the desired result. \square

Lemma 4. If z_A and \tilde{z}_A are as in Lemma 3, one has

$$|\tilde{z}_A - z_A| \lesssim \left(\sum_{T' \in \tilde{\mathcal{T}}_h^h(T)} \|\nabla z_h\|_{0,T'}^2 \right)^{1/2}.$$

Proof. We recall that $\tilde{\mathcal{T}}_h^h(T)$ be the set of triangles in $\tilde{\Omega}_h$ whose vertices influence the definition of the extension operator E_h on the triangle T . We split the proof in the case of the gradient-based extension and the moving least-square extension:

Gradient-based extension. We have

$$\tilde{z}_A = \sum_{B \in \tilde{\mathcal{N}}_A} \alpha_{AB} (z_B + (\tilde{\mathbf{G}}z_h)_B \cdot e_{BA}).$$

and

$$z_A = \underbrace{\sum_{B \in \tilde{\mathcal{N}}_A} \alpha_{AB} z_A}_{=1} = \sum_{B \in \tilde{\mathcal{N}}_A} \alpha_{AB} (z_B + \nabla z_h|_{T_{AB}} \cdot e_{BA}),$$

where $\nabla z_h|_{T_{AB}}$ is the gradient measured on either of the elements that share the edge e_{BA} (observe that the gradients on either element have the same projection along e_{BA}). Hence

$$\tilde{z}_A - z_A = \sum_{B \in \tilde{\mathcal{N}}_A} \alpha_{AB} \left((\tilde{\mathbf{G}}z_h)_B - \nabla z_h|_{T_{AB}} \right) \cdot e_{BA}$$

and

$$|\tilde{z}_A - z_A|^2 \leq \sum_{B \in \tilde{\mathcal{N}}_A} \|(\tilde{\mathbf{G}}z_h)_B - \nabla z_h|_{T_{AB}}\|^2 \|e_{BA}\|^2 \lesssim \sum_{T \in \tilde{\mathcal{T}}_{h:A}} \|\nabla z_h|_T\|^2 h_T^2 \simeq \sum_{T \in \tilde{\mathcal{T}}_{h:A}} \|\nabla z_h|_T\|_{0,T}^2.$$

Moving least-square extension. In this case, in view of (19) and Remark 4, we have

$$|\tilde{z}_A - z_A| = \sum_{B \in \mathcal{N}_A^{MLS}} \omega_{AB} |z_B - z_A|,$$

and $|z_B - z_A|$ can be bound by the sum of gradients of z_h as done in the proof of Lemma 1 (for the moving least-square case). \square

Now we can proceed to bound (28), as summarized in the following result:

Corollary 7. Assume that $w \in H^2(\tilde{\Omega}_h^+)$, where $\tilde{\Omega}_h^+ = \tilde{\Omega}_h \cup \Omega_h^f$. Then

$$\|h^{1/2}(\mathbb{E}_h w - w)\|_{0,\Gamma} \lesssim h_{\tilde{\Gamma}_h}^2 |w|_{2,\tilde{\Omega}_h^+},$$

with $h_{\tilde{\Gamma}_h} = \max\{h_T : T \cap \tilde{\Gamma}_h \neq \emptyset\}$.

Proof. Consider an element in $T \subset \Omega_h^f$. Then

$$h_T^{1/2} \|\mathbb{E}_h w - w\|_{0,T \cap \Gamma} \lesssim \|\mathbb{E}_h w - w\|_{0,T} + h_T \|\nabla(\mathbb{E}_h w - w)\|_{0,T} \tag{29}$$

and

$$\|\nabla(\mathbb{E}_h w - w)\|_{0,T} \lesssim \|\nabla(\mathbb{E}_h w - \mathbb{I}_h w)\|_{0,T} + \|\nabla(\mathbb{I}_h w - w)\|_{0,T} \lesssim h_T^{-1} \|\mathbb{E}_h w - \mathbb{I}_h w\|_{0,T} + h_T |w|_{2,T}, \tag{30}$$

where $\mathbb{E}_h w - \mathbb{I}_h w \in \mathcal{P}^1(T)$. Substituting (30) into (29), we have

$$h_T^{1/2} \|\mathbb{E}_h w - w\|_{0,T \cap \Gamma} \lesssim 2\|\mathbb{E}_h w - \mathbb{I}_h w\|_{0,T} + \|w - \mathbb{I}_h w\|_{0,T} + h_T^2 |w|_{2,T} \lesssim \|\mathbb{E}_h w - \mathbb{I}_h w\|_{0,T} + h_T^2 |w|_{2,T}$$

Now observe that for an arbitrary $\tau \in \mathcal{P}^1(T)$, we have $\mathbb{E}_h \tau = \tau$ (for both the gradient-based and moving least-squares extension operators) and $\mathbb{I}_h \tau = \tau$. Hence, setting $z = w - \tau$, we have $\mathbb{E}_h w - \mathbb{I}_h w = \mathbb{E}_h z - \mathbb{I}_h z$ and, using Lemmas 3 and 4:

$$\|\mathbb{E}_h w - \mathbb{I}_h w\|_{0,T} = \|\mathbb{E}_h z - \mathbb{I}_h z\|_{0,T} \lesssim h_T \left(\sum_{T' \in \mathcal{T}_h^h(T)} \|\nabla(\mathbb{I}_h z)\|_{0,T'}^2 \right)^{1/2}.$$

Now

$$\|\nabla(\mathbb{I}_h z)\|_{0,T'} \leq \|\nabla z\|_{0,T'} + \|\nabla(z - \mathbb{I}_h z)\|_{0,T'}$$

with

$$\|\nabla(z - \mathbb{I}_h z)\|_{0,T'} = \|\nabla(w - \mathbb{I}_h w)\|_{0,T'} \lesssim h_{T'} |w|_{2,T'}.$$

Let us set now $\mathcal{S}(T) = \bigcup\{T' \in \mathcal{T}_h^h(T)\}$ and observe that $\text{diam}(\mathcal{S}(T)) \simeq h_T \simeq h_{T'}, \forall T' \in \mathcal{T}_h^h(T)$, since only a finite number of elements, independent of h , belongs to $\mathcal{T}_h^h(T)$. Hence

$$\left(\sum_{T' \in \mathcal{T}_h^h(T)} \|\nabla(\mathbb{I}_h z)\|_{0,T'}^2 \right)^{1/2} = \|\nabla z\|_{0,\mathcal{S}(T)} = \|\nabla(w - \tau)\|_{0,\mathcal{S}(T)}$$

and choosing τ as the projection of w upon $\mathcal{P}^1(\mathcal{S}(T))$ in the gradient norm, we have

$$\|\nabla(w - \tau)\| \lesssim h_T |w|_{2,\mathcal{S}(T)} \simeq \left(\sum_{T' \in \mathcal{T}_h^h(T)} (h_{T'} |w|_{2,T'})^2 \right)^{1/2}.$$

In conclusion,

$$\|\mathbb{E}_h w - \mathbb{I}_h w\|_{0,T} \lesssim \left(\sum_{T' \in \mathcal{T}_h^h(T)} (h_{T'} |w|_{2,T'})^2 \right)^{1/2},$$

which completes the proof. \square

6. Numerical analysis of the method for the Poisson equation

In what follows, we perform the numerical analysis of the proposed method. Under a number of technical assumptions, we prove numerical stability, continuity, asymptotic consistency, and optimal convergence of the variational formulation in the natural norm. These are the main results discussed next and a reader more interested in the actual numerical performance of the proposed approach can skip this section and move directly to Sections 4 and 7.

6.1. Well-posedness and stability

In the proofs of numerical stability and convergence that follow, we will make the following technical assumptions.

Assumption 2. The boundary conditions in problem (6) are only of Dirichlet type, that is $\Gamma \equiv \Gamma_D$.

Assumption 3. For some arbitrarily small $\zeta \in \mathbb{R}^+$, it holds

$$|\mathbf{d}| \sim h^{1+\zeta}. \tag{31}$$

Remark 7. Assumption 3 will not be used in numerical computations, but is simply confined to the mathematical proofs. For example, when nested grid refinement is employed, then $\zeta = 0$ in Assumption 3. The condition $\zeta > 0$ implies that the grids are adapted after every refinement so that $\tilde{\Gamma}_h$ is pushed slightly towards Γ .

Under Assumption 2, (6) reduces to:

Find $u_h \in V_h(\tilde{\Omega}_h)$ such that,

$$a_h(u_h, w_h) = l_h(w_h), \quad \forall w_h \in V_h(\tilde{\Omega}_h), \tag{32a}$$

where

$$a_h(u_h, w_h) = (\nabla u_h, \nabla w_h)_{\tilde{\Omega}_h} - \langle \nabla u_h \cdot \tilde{\mathbf{n}}, w_h \rangle_{\tilde{\Gamma}_h} - \langle \mathbf{E}_h u_h, \nabla(\mathbf{E}_h w_h) \cdot \tilde{\mathbf{n}} - \alpha h_{\perp}^{-1} \mathbf{E}_h w_h \rangle_{\Gamma}, \tag{32b}$$

$$l_h(w_h) = (f, w_h)_{\tilde{\Omega}_h} - \langle g, \nabla(\mathbf{E}_h w_h) \cdot \tilde{\mathbf{n}} - \alpha h_{\perp}^{-1} \mathbf{E}_h w_h \rangle_{\Gamma}. \tag{32c}$$

Remark 8. Because of the use of the extension operator \mathbf{E}_h , the bilinear form $a_h(u_h, w_h)$ is not symmetric.

As a first step, we prove that the proposed method is stable, by a coercivity argument.

Theorem 2 (Coercivity). Consider the bilinear form $a_h(u_h, w_h)$ defined in (32), under Assumptions 1, 2, and 3. Then, for α sufficiently large, there exists a constant $C_a > 0$, independent of the mesh size, such that

$$a_h(u_h, u_h) \geq C_a \|u_h\|_a^2 \quad \forall u_h \in V_h(\tilde{\Omega}_h), \tag{33}$$

where $\|u_h\|_a$ was defined in (27).

Proof. By substitution, we have

$$a_h(u_h, u_h) = \|\nabla u_h\|_{0, \tilde{\Omega}_h}^2 - \langle \nabla u_h \cdot \tilde{\mathbf{n}}, u_h \rangle_{\tilde{\Gamma}_h} - \langle \mathbf{E}_h u_h, \nabla(\mathbf{E}_h u_h) \cdot \mathbf{n} \rangle_{\Gamma} + \alpha \|h^{-1/2} \mathbf{E}_h u_h\|_{0, \Gamma}^2. \tag{34}$$

From Cauchy's inequality, Young's ϵ -inequality, we obtain

$$\begin{aligned} a_h(u_h, u_h) &\geq \|\nabla u_h\|_{0, \tilde{\Omega}_h}^2 - \frac{\epsilon_1}{2} \|h^{1/2} \nabla u_h \cdot \tilde{\mathbf{n}}\|_{0, \tilde{\Gamma}_h}^2 - \frac{\epsilon_1^{-1}}{2} \|h^{-1/2} u_h\|_{0, \tilde{\Gamma}_h}^2 \\ &\quad - \frac{\epsilon_2}{2} \|h^{1/2} \nabla(\mathbf{E}_h u_h) \cdot \mathbf{n}\|_{0, \Gamma}^2 - \frac{\epsilon_2^{-1}}{2} \|h^{-1/2} \mathbf{E}_h u_h\|_{0, \Gamma}^2 + \alpha \|h^{-1/2} \mathbf{E}_h u_h\|_{0, \Gamma}^2. \end{aligned} \tag{35}$$

Corollary 4 then yields

$$\begin{aligned} a_h(u_h, u_h) &\geq \|\nabla u_h\|_{0, \tilde{\Omega}_h}^2 - \frac{\epsilon_1}{2} \|h^{1/2} \nabla u_h \cdot \tilde{\mathbf{n}}\|_{0, \tilde{\Gamma}_h}^2 - \frac{\hat{c}_{\otimes}}{2\epsilon_1} \left(\|h^{-1/2} \mathbf{E}_h u_h\|_{0, \Gamma}^2 + \max_{T \in \Omega_h^T} \left(\frac{\max_{T \cap \tilde{\Gamma}_h} |\mathbf{d}|}{h_T} \right) \|\nabla u_h\|_{0, \tilde{\Omega}_h}^2 \right) \\ &\quad - \frac{\epsilon_2}{2} \|h^{1/2} \nabla(\mathbf{E}_h u_h) \cdot \mathbf{n}\|_{0, \Gamma}^2 - \frac{\epsilon_2^{-1}}{2} \|h^{-1/2} \mathbf{E}_h u_h\|_{0, \Gamma}^2 + \alpha \|h^{-1/2} \mathbf{E}_h u_h\|_{0, \Gamma}^2. \end{aligned} \tag{36}$$

The discrete trace inequality (A.4b) in Appendix, Corollary 2, and the definition of the norm $\|\cdot\|_a$ yield

$$\begin{aligned} a_h(u_h, u_h) &\geq \left(1 - \tilde{C}_I \frac{\epsilon_1}{2} - c \cdot \frac{\epsilon_2}{2} - \frac{\hat{c}_{\otimes}}{2\epsilon_1} \max_{T \in \Omega_h^T} \left(\frac{\max_{T \cap \tilde{\Gamma}_h} |\mathbf{d}|}{h_T} \right) \right) \|\nabla u_h\|_{0, \tilde{\Omega}_h}^2 + \left(\alpha - \frac{1}{2\epsilon_1} - \frac{1}{2\epsilon_2} \right) \|h^{-1/2} \mathbf{E}_h u_h\|_{0, \Gamma}^2 \\ &\geq \min \left(1 - \tilde{C}_I \frac{\epsilon_1}{2} - c \cdot \frac{\epsilon_2}{2} - \frac{\hat{c}_{\otimes}}{2\epsilon_1} \max_{T \in \Omega_h^T} \left(\frac{\max_{T \cap \tilde{\Gamma}_h} |\mathbf{d}|}{h_T} \right), \alpha - \frac{1}{2\epsilon_1} - \frac{1}{2\epsilon_2} \right) \|u_h\|_a^2. \end{aligned} \tag{37}$$

Taking now $\epsilon_1 = 1/(3\tilde{C}_I)$, $\epsilon_2 = 1/(3c)$, $\alpha = 1/2 + 3/2(\tilde{C}_I + c)$ and observing that, by Assumption 3, for a sufficiently refined grid, $\max_{T \in \Omega_h^T} (h_T^{-1} \max_{T \cap \tilde{\Gamma}_h} |\mathbf{d}|) < (9\hat{c}_{\otimes} \tilde{C}_I)^{-1}$, we obtain the asymptotic coercivity statement (33) with $C_a = 1/2$. \square

6.2. Consistency and convergence analysis

From now on, we pose the following regularity assumption on the exact solution u of our Dirichlet problem (see [49,56]):

Assumption 4. Assume that Γ is of class \mathcal{C}^2 , $f \in L^2(\Omega)$ and $u_D \in H^{3/2}(\Gamma)$.

As a consequence, **Theorem 1** guarantees $u \in H^2(\Omega)$ with the estimate (5). Actually, u can be extended to a function, still denoted by u , which belongs to $H^2(\tilde{\Omega}_h^+)$ and satisfies

$$\|u\|_{2,\tilde{\Omega}_h^+} \leq C (\|f\|_{0,\Omega} + \|u_D\|_{3/2,\Gamma}). \quad (38)$$

See, for more details [57]. This assumption allows us to keep technicalities at a minimum in the subsequent consistency and convergence analysis. Note however that it can be weakened to include domains with a finite number of corners and/or edges (see [49,56]).

Observe that the bilinear form $a_h(\cdot, \cdot)$ is well-defined also on the space $V(\tilde{\Omega}_h; \tilde{\mathcal{T}}_h) \times V_h(\tilde{\Omega}_h)$ introduced in Section 5.4.1. The proof of convergence of the SBM for Problem (4) using the natural norm $\|\cdot\|_a$ defined in (27), relies on Strang's Second Lemma, stated without proof, as it is classic [50]:

Lemma 5 (Strang's Second Lemma). *If $u_h \in V_h(\tilde{\Omega}_h)$ is the solution of (32), then*

$$\|u - u_h\|_{V(\tilde{\Omega}_h; \tilde{\mathcal{T}}_h)} \leq \left(1 + C_a^{-1} \|a_h\|_{V_h(\tilde{\Omega}_h) \times V_h(\tilde{\Omega}_h)}\right) E_{a,h}(u) + C_a^{-1} E_{c,h}(u). \quad (39a)$$

where

$$E_{a,h}(u) = \inf_{w_h \in V_h(\tilde{\Omega}_h)} \|u - w_h\|_{V(\tilde{\Omega}_h; \tilde{\mathcal{T}}_h)} \quad (39b)$$

is the approximation error and

$$E_{c,h}(u) = \sup_{w_h \in V_h(\tilde{\Omega}_h)} \frac{|l_h(w_h) - a_h(u, w_h)|}{\|w_h\|_{V(\tilde{\Omega}_h; \tilde{\mathcal{T}}_h)}} \quad (39c)$$

is the consistency error.

From **Theorem 2**, we already have that C_a is a constant independent of the mesh size. Hence, to estimate the discretization error in the norm $\|\cdot\|_{V(\tilde{\Omega}_h; \tilde{\mathcal{T}}_h)}$ we need to prove that $\|a_h\|_{V_h(\tilde{\Omega}_h) \times V_h(\tilde{\Omega}_h)}$ is bounded from above and to estimate the approximation and consistency errors in terms of the mesh size $h_{\tilde{\Omega}_h}$. Recalling the notation at the beginning of Section 5.4.1, we have the following result:

Proposition 1 (Boundedness). *There exists a constant $C_{\mathcal{B}} > 0$, independent of the mesh size, such that*

$$a_h(u, w) \leq C_{\mathcal{B}} \|u\|_{V(\tilde{\Omega}_h; \tilde{\mathcal{T}}_h)} \|w\|_{V(\tilde{\Omega}_h; \tilde{\mathcal{T}}_h)}, \quad \forall u, w \in V(\tilde{\Omega}_h; \tilde{\mathcal{T}}_h). \quad (40)$$

Proof. Using the Cauchy–Schwartz inequality we obtain:

$$\begin{aligned} a_h(u, w) &= (\nabla u, \nabla w)_{\tilde{\Omega}_h} - \langle \nabla u \cdot \tilde{\mathbf{n}}, w \rangle_{\tilde{\Gamma}_h} - \langle \mathbf{E}_h u, \nabla(\mathbf{E}_h w) \cdot \mathbf{n} \rangle_{\Gamma} + \langle \mathbf{E}_h u, \alpha h_{\perp}^{-1} \mathbf{E}_h w \rangle_{\Gamma} \\ &\leq \|\nabla u\|_{0,\tilde{\Omega}_h} \|\nabla w\|_{0,\tilde{\Omega}_h} + \|h^{1/2} \nabla u \cdot \tilde{\mathbf{n}}\|_{0,\tilde{\Gamma}_h} \|h^{-1/2} w\|_{0,\tilde{\Gamma}_h} + \|h^{-1/2} \mathbf{E}_h u\|_{0,\Gamma} \|h^{1/2} \nabla(\mathbf{E}_h w) \cdot \mathbf{n}\|_{0,\Gamma} \\ &\quad + \alpha \|h^{-1/2} \mathbf{E}_h u\|_{0,\Gamma} \|h^{-1/2} \mathbf{E}_h w\|_{0,\Gamma}, \end{aligned} \quad (41)$$

Using now the scale trace inequality (A.3b) in **Theorem 6** of **Appendix** and **Corollaries 5** and **6**, we obtain

$$\begin{aligned} a_h(u, w) &\lesssim \|\nabla u\|_{0,\tilde{\Omega}_h} \|\nabla w\|_{0,\tilde{\Omega}_h} + C_I \|u\|_{V(\tilde{\Omega}_h; \tilde{\mathcal{T}}_h)} \left(\|h^{-1/2} \mathbf{E}_h w\|_{0,\Gamma}^2 + \left(1 + \max_{T \in \tilde{\mathcal{T}}_h} \left(\frac{\max_{T \cap \tilde{\Gamma}_h} |\mathbf{d}|}{h_T}\right)\right) \|w\|_{V(\tilde{\Omega}_h; \tilde{\mathcal{T}}_h)} \right) \\ &\quad + \|h^{-1/2} \mathbf{E}_h u\|_{0,\Gamma} \|w\|_{V(\tilde{\Omega}_h; \tilde{\mathcal{T}}_h)} + \alpha \|h^{-1/2} \mathbf{E}_h u\|_{0,\Gamma} \|h^{-1/2} \mathbf{E}_h w\|_{0,\Gamma} \\ &\lesssim \|u\|_{V(\tilde{\Omega}_h; \tilde{\mathcal{T}}_h)} \|w\|_{V(\tilde{\Omega}_h; \tilde{\mathcal{T}}_h)}, \end{aligned} \quad (42)$$

which can be restated by saying that there exists a positive constant $C_{\mathcal{B}}$, independent of the mesh size, such that

$$\|a_h\|_{V(\tilde{\Omega}_h; \tilde{\mathcal{T}}_h) \times V(\tilde{\Omega}_h; \tilde{\mathcal{T}}_h)} = \sup_{u \in V(\tilde{\Omega}_h; \tilde{\mathcal{T}}_h)} \sup_{w \in V(\tilde{\Omega}_h; \tilde{\mathcal{T}}_h)} \frac{a_h(u, w)}{\|u\|_{V(\tilde{\Omega}_h; \tilde{\mathcal{T}}_h)} \|w\|_{V(\tilde{\Omega}_h; \tilde{\mathcal{T}}_h)}} \leq C_{\mathcal{B}}. \quad \square \quad (43)$$

Proposition 2 (Approximability). *There exists a constant $C_{\mathcal{A}} > 0$, independent of the mesh size, such that*

$$E_{a,h}(u) \leq C_{\mathcal{A}} h_{\tilde{\Omega}_h} |u|_{2,\tilde{\Omega}_h}, \quad \forall u \in V(\tilde{\Omega}_h; \tilde{\mathcal{T}}_h), \quad (44)$$

where $h_{\tilde{\Omega}_h}$ is the maximum h_T for $T \subset \tilde{\Omega}_h$.

Proof. Let $w_h = l_h u$ in (39b), where $l_h u$ is the standard piecewise-linear Lagrange interpolate of u on the triangulation $\tilde{\mathcal{T}}_h$. Consequently, the goal is to estimate

$$\begin{aligned} \|u - l_h u\|_{V(\tilde{\Omega}_h; \tilde{\mathcal{T}}_h)} &= \|\nabla(u - l_h u)\|_{0,\tilde{\Omega}_h} + \|h^{-1/2} \mathbf{E}_h(u - l_h u)\|_{0,\Gamma} + |h(u - l_h u)|_{2,\tilde{\Omega}_h; \tilde{\mathcal{T}}_h} \\ &\leq \|\nabla(u - l_h u)\|_{0,\tilde{\Omega}_h} + \|h^{-1/2} \mathbf{E}_h(u - l_h u)\|_{0,\Gamma} + h_{\tilde{\Omega}_h} |u|_{2,\tilde{\Omega}_h}. \end{aligned} \quad (45)$$

We begin by stating a classical interpolation result

$$\|h^{-1}(u - I_h u)\|_{0,\tilde{\Omega}_h} + \|\nabla(u - I_h u)\|_{0,\tilde{\Omega}_h} \leq C_1 h_{\tilde{\Omega}_h} |u|_{2,\tilde{\Omega}_h}, \tag{46}$$

where C_1 is a positive constant independent of the mesh size, and we also observe that $\|h^{-1/2} E_h(u - I_h u)\|_{0,\Gamma} = 0$, by Definition 4. Replacing (46) in (45) gives (44) with $C_{\mathcal{A}} = 1 + C_1$. \square

Proposition 3 (Consistency Error). *There exists a constant $C_{\mathcal{E}} > 0$ independent of the mesh size and u such that*

$$E_{c,h}(u) \leq C_{\mathcal{E}} h_{\tilde{\Gamma}_h} |u|_{2,\tilde{\Omega}_h^+}. \tag{47}$$

Proof. Integrating by parts the bilinear form $a_h(\cdot, \cdot)$ given in (32b) and applying Corollary 7 yields

$$\begin{aligned} |a_h(u, w_h) - I_h(w_h)| &= | - \langle E_h u - u + \underbrace{u - g}_{=0}, \nabla(E_h w_h) \cdot \tilde{\mathbf{n}} - \alpha h_{\perp}^{-1} E_h w_h \rangle_{\Gamma} | \\ &\leq | \langle E_h u - u, \nabla(E_h w_h) \cdot \tilde{\mathbf{n}} \rangle_{\Gamma} | + | \langle E_h u - u, \alpha h_{\perp}^{-1} E_h w_h \rangle_{\Gamma} | \\ &\leq \|h^{-1/2}(E_h u - u)\|_{0,\Gamma} (\|h^{1/2} \nabla(E_h w_h) \cdot \mathbf{n}\|_{0,\Gamma} + \|\alpha h^{-1/2} E_h w_h\|_{0,\Gamma}) \\ &\lesssim h_{\tilde{\Gamma}_h} |u|_{2,\tilde{\Omega}_h^+} \|w_h\|_{V(\tilde{\Omega}_h; \tilde{\mathcal{F}}_h)}. \end{aligned} \tag{48}$$

The proof is concluded by replacing (48) in (39c). \square

Theorem 3 (Convergence in the Natural Norm). *Under Assumption 4 and the condition that $h_{\tilde{\Gamma}_h}$ is sufficiently small, the numerical solution u_h of the SBM (6) satisfies the following error estimate:*

$$\|u - u_h\|_{V(\tilde{\Omega}_h; \tilde{\mathcal{F}}_h)} \leq C h_{\tilde{\Omega}_h} (\|f\|_{0,\Omega} + \|u_D\|_{3/2,\Gamma}), \tag{49}$$

where u is the exact solution of Problem (4) and $C > 0$ is a constant independent of the mesh size and the solution.

Proof. Combining Strang’s abstract error estimate (39a) with the stability bound (33), the error estimates in Propositions 2 and 3, and the regularity estimate (38) gives (49). \square

7. Numerical studies

We consider a series of two-dimensional tests to verify the main theoretical results obtained in the previous sections.

7.1. Poisson problem on an annulus

The computational domain is an annulus of inner radius $a = 1$ and outer radius $b = 3$. Strong Dirichlet conditions are applied on the outer boundary, which is body-fitted (i.e., the nodes of the grid lie on the true boundary Γ), while weak SBM boundary conditions of Dirichlet or Neumann type are applied on the inner boundary, which is immersed.

The exact solution \bar{u} to this problem is generated with the method of manufactured solutions, by applying an appropriate forcing term f compatible with the following analytical expression:

$$\bar{u}(x, y) = \frac{1}{4} (9 - x^2 - y^2 - 2 \ln 3 + \ln(x^2 + y^2)) + \frac{1}{4} \sin x \sinh y.$$

7.1.1. Extension operator consistency and accuracy

This preliminary test aims at verifying the accuracy and consistency of the extension operators. In this test, the values of the exact solution \bar{u} are initially imposed at all the nodes in $\tilde{\Omega}_h$ and the two versions of the extension operator E_h are combined with formulas (13) and (14), to compute $E_h \bar{u}$ on $\tilde{\Gamma}_h$. The quality of the extension operators is quantified with the L^2 -norm of the error $\|E_h \bar{u} - \bar{u}\|_{0,\Gamma}$ and the H^1 -seminorm of the error $|E_h \bar{u} - \bar{u}|_{1,\Gamma}$, both evaluated over Γ .

Fig. 7 depicts the convergence of the L^2 -error on the boundary Γ for the two variants of the extension operator.

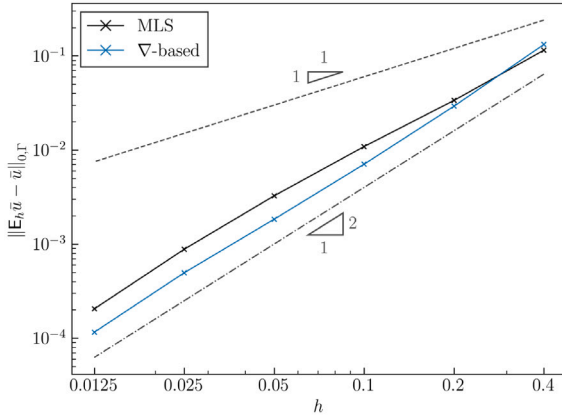
Both the MLS and the average gradient extensions feature optimal, quadratic convergence rate, with slightly lower errors for the average gradient extension (see Fig. 7(a)). A similar behavior is observed for the H^1 -seminorm of the errors (see Fig. 7(b)), which show optimal, linear convergence rates.

7.1.2. Dirichlet and Neumann boundary conditions convergence

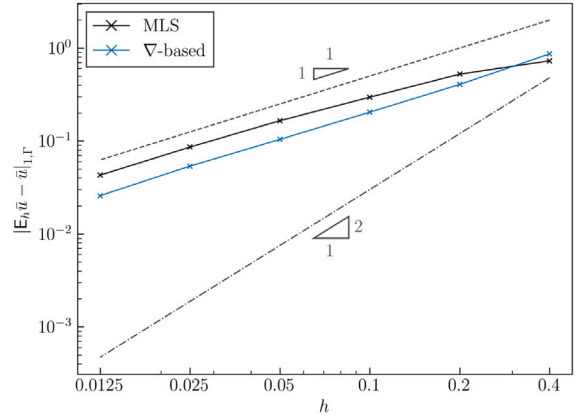
In this test we assess the convergence rate of the L^2 -error $\|u - \bar{u}\|_{L^2(\tilde{\Omega}_h)}$ (computed over $\tilde{\Omega}_h$), when imposing Dirichlet and Neumann boundary conditions.

We present the results obtained with formulation (6), as well as the mixed formulation of the Poisson Eq. (9).

Fig. 8 depicts the results obtained when enforcing a Dirichlet boundary condition in the inner boundary of the annulus, with a penalty parameter $\alpha = 10.0$. The proposed method exhibits optimal quadratic convergence of the L^2 -norm of the error, for both the MLS and the average gradient extension operators. Convergence is also optimal (first-order) for the H^1 -seminorm of the error, as shown in Fig. 9. Figs. 8 and 9 also demonstrate that similar results are obtained with the mixed form (9).

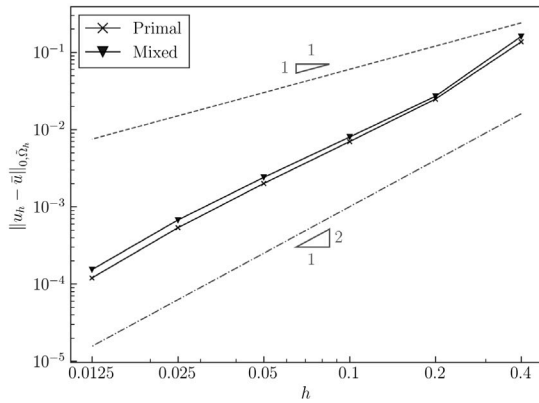


(a) L^2 -norm of the error.

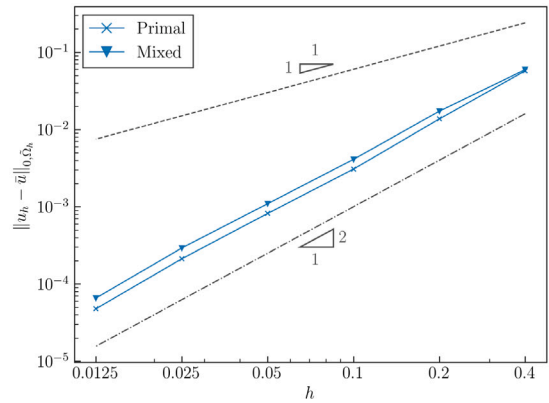


(b) H^1 -seminorm of the error.

Fig. 7. Accuracy test of the extension operators (annulus geometry). Convergence of the error norms for MLS and average gradient (labeled as ∇ -based) extension operators, for a given analytical solution field on Ω_h . Dashed and dash-dotted lines represent linear and quadratic convergence rates, respectively.



(a) MLS extension operator.



(b) Average gradient extension operator.

Fig. 8. Poisson problem on an annulus domain with an unfitted Dirichlet boundary condition. Convergence of the L^2 -norm of the error, $\|u_h - \bar{u}\|_{0,\Omega_h}$, for the MLS and average gradient extension operators. Results are presented for primal (irreducible) and mixed formulations. Dashed and dash-dotted lines represent linear and quadratic convergence rates.

Fig. 10 shows the convergence results when Neumann boundary conditions are imposed over the inner boundary of the annulus. In this case, the L^2 -error of the solution obtained with the irreducible formulation (6) is only first-order accurate, for both variants of the extension operator. Quadratic convergence rates are reestablished using the mixed-form of the variational Eqs. (9) in conjunction with the MLS extension (see **Fig. 10(a)**), but not the average gradient extension (see **Fig. 10(b)**). The H^1 -seminorms of the error converge optimally for both irreducible and mixed formulations and both types of extension, as shown in **Fig. 11**.

7.2. Poisson problem on a trapezoidal plate

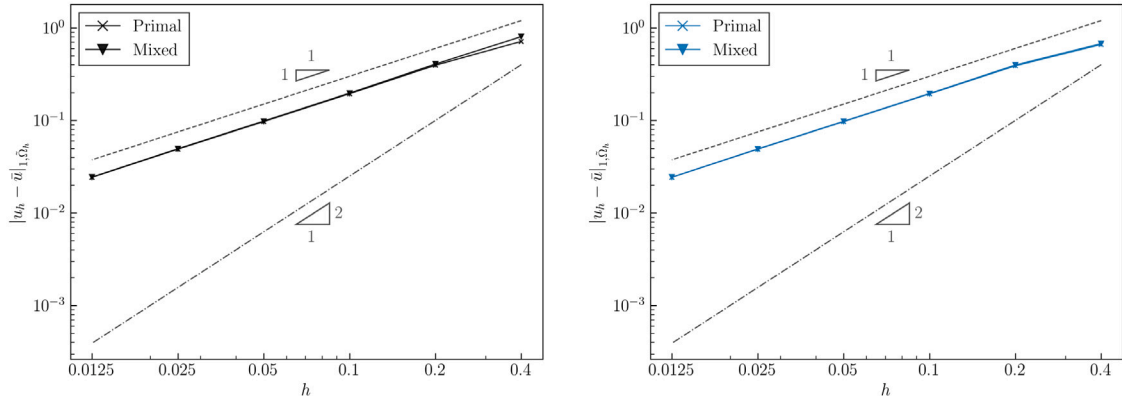
This test was originally presented in [56] and is very well suited to prove that the proposed method is not affected by irregular grid patterns in the surrogate boundary. The computational domain Ω (**Fig. 12**) consists of a right trapezoid with unit height ($s = 1.0$), top side of length $b_1 = 0.6$, and bottom side of length $b_2 = 0.4$. The exact solution

$$\bar{u}(x, y) = y \sin(2\pi x) - x \cos(2\pi y),$$

is enforced using the method of manufactured solutions, by enforcing the source term

$$f(x, y) = 4\pi^2 (y \sin(2\pi x) - x \cos(2\pi y)).$$

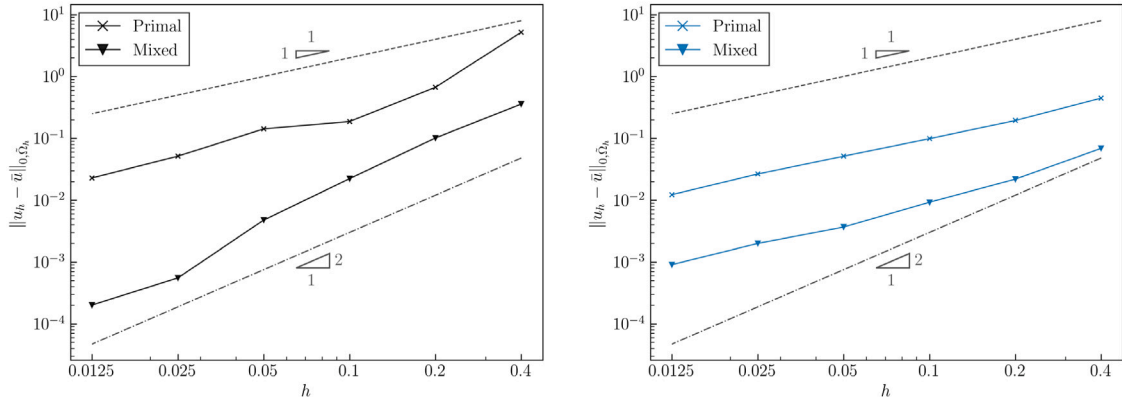
In order to create irregular patterns in the surrogate grid, we start by meshing the trapezoid with rectangular (quadrilateral) elements of aspect ratio 5:1, which are subsequently divided into four triangular elements each. Hence the top, left, and bottom sides of the



(a) MLS extension operator.

(b) Average gradient extension operator.

Fig. 9. Poisson problem on an annulus domain with an unfitted Dirichlet boundary condition. Convergence of the H^1 -seminorm of the error, $\|u_h - \bar{u}\|_{1, \Omega_h}$, for the MLS and average gradient extension operators. Results are presented for primal (irreducible) and mixed formulations. Dashed and dash-dotted lines represent linear and quadratic convergence rates.



(a) MLS extension operator.

(b) Average gradient extension operator.

Fig. 10. Poisson problem on an annulus domain with an unfitted Neumann boundary condition. Convergence of the L^2 -norm of the error, $\|u_h - \bar{u}\|_{0, \Omega_h}$, for the MLS and average gradient extension operators. Results are presented for primal (irreducible) and mixed formulations. Dashed and dash-dotted lines represent linear and quadratic convergence rates.

trapezoid are meshed with a body fitted grid, while the right (oblique) side is immersed. The location of the oblique side is slightly displaced according to the following definition of the distance function:

$$d(x, y) = \text{sgn}(\bar{d}) \left| \max(\bar{d}, \varepsilon_d) \right|,$$

where \bar{d} will be defined momentarily, and $\varepsilon_d = 10^{-12}$. Assuming that the bottom left corner of the trapezoid is placed at $(-0.5, -0.5)$ in the reference coordinates, \bar{d} is given by

$$\bar{d}(x, y) = -\frac{5x - y}{26}.$$

Dirichlet conditions are applied on the entire boundary. The computational results, described in Fig. 13 show optimal convergence of the L^2 -error for both the MLS and average gradient extension operators.

7.3. Compressible Cook's membrane

This last example extends the previous results to the case of compressible linear elasticity, using the formulation described in Section 4 to solve the classical compressible Cook's membrane benchmark.

The problem geometry and material properties are described in Fig. 14. The Young modulus and Poisson ratio are equal to 200 N/mm² and 0.3, respectively. The problem is solved for a set of "structured" triangular meshes with size ranging from 0.75 mm to

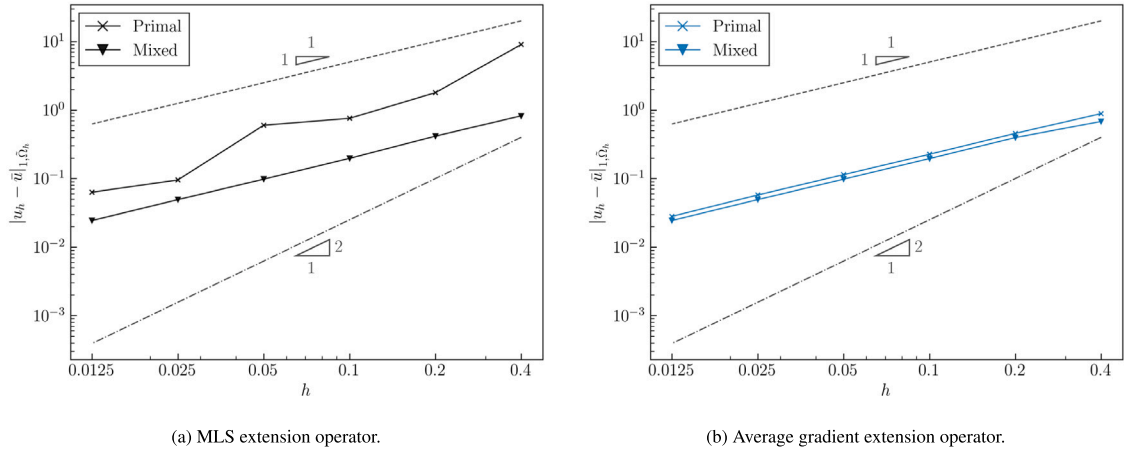


Fig. 11. Poisson problem on an annulus domain with an unfitted Neumann boundary condition. Convergence of the H^1 -seminorm of the error, $|u_h - \bar{u}|_{1, \tilde{\Omega}_h}$, for the MLS and average gradient extension operators. Results are presented for primal (irreducible) and mixed formulations. Dashed and dash-dotted lines represent linear and quadratic convergence rates.

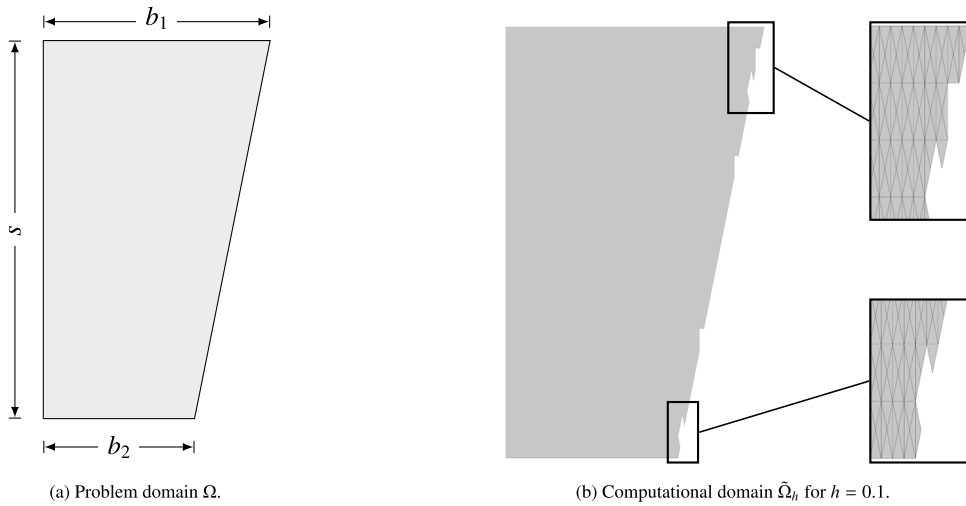


Fig. 12. Problem domain Ω .

12 mm. These grids are fitted to all sides of the membrane except the left vertical side, which is immersed. A vertical (tangential) distributed load of 0.00625 N/mm^2 is applied along the vertical right side of the membrane. Zero displacement is enforced on the left vertical side, using the proposed unfitted method.

Since there is no analytical solution for this problem, we compare the results obtained with the proposed immersed method against a reference solution obtained with a body-fitted grid and a piecewise-linear finite element formulation. The element size of the body-fitted grid is chosen to be less than one tenth of the element size of the finest immersed grid used. Fig. 15 shows the L^2 -norm and H^1 -seminorm of the error, both converging with optimal rates.

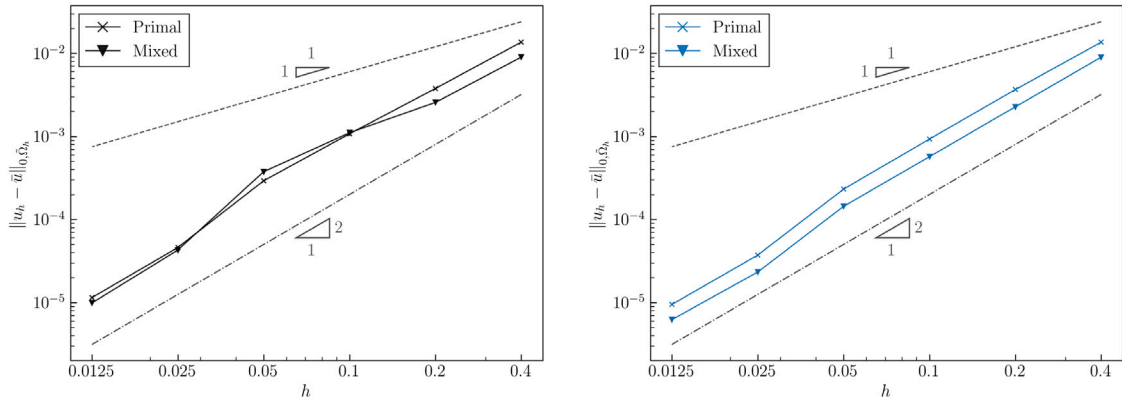
8. Summary

We introduced and analyzed a new variant of the SBM method that utilizes general extension operators rather than Taylor expansions to shift the location where boundary conditions are applied.

In particular, we analyzed how the properties of the extension operators affect the numerical stability and convergence of the overall shifted formulation.

We considered two variants of the extension operator, one based on averaging the gradient of the solution on a patch of elements near the surrogate boundary, and another based on a Moving Least Square technique.

Both approaches were tested in the context of the Laplace equation and the equations of compressible linear elasticity, in the case of Dirichlet and Neumann conditions.



(a) MLS extension operator.

(b) Average gradient extension operator.

Fig. 13. Poisson problem on a trapezoidal plate. Convergence of the $\|u_h - \bar{u}\|_{0,\hat{\Omega}_h}$ error norms for MLS and average gradient extension operators. Results are presented for primal (irreducible) and mixed formulations. Dashed and dash-dotted lines represent linear and quadratic convergence rates.

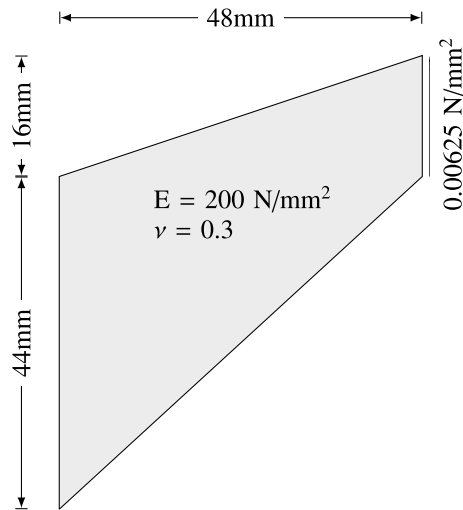
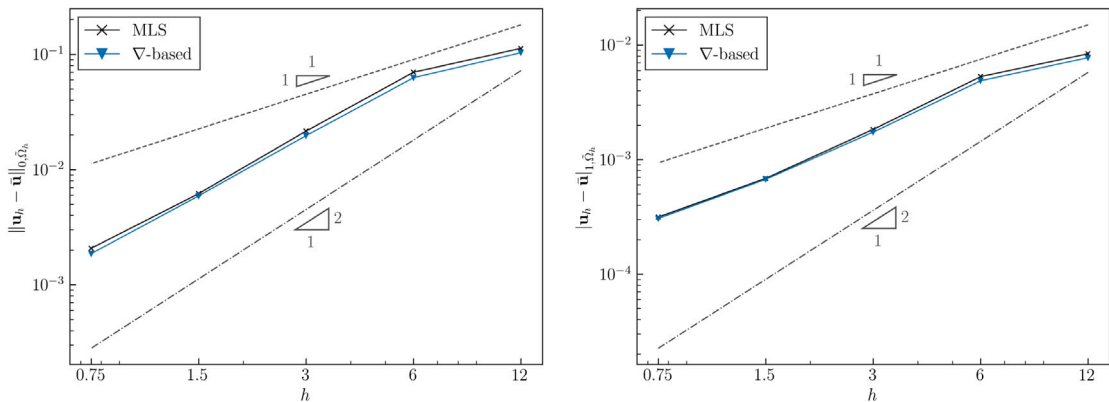


Fig. 14. Compressible Cook's membrane. Geometry, load and material properties.



(a) L^2 -norm of the error: $\|u_h - \bar{u}\|_{0,\hat{\Omega}_h}$.

(b) H^1 -seminorm of the error: $|u_h - \bar{u}|_{1,\hat{\Omega}_h}$.

Fig. 15. Compressible Cook's membrane. Error norms for MLS and average gradient (labeled as ∇ -based) extension operators. Dashed and dash-dotted lines represent linear and quadratic convergence rates.

Future research will be directed in the context of computational fluid dynamics and IsoGeometric Analysis (IGA), including the extension of the proposed method to thin-walled (i.e. shell-like) structures.

Declaration of competing interest

The authors declare that they have no known competing financial interests or personal relationships that could have appeared to influence the work reported in this paper.

Data availability

Data will be made available on request.

Acknowledgments

This research is partly supported by the European High-Performance Computing Joint Undertaking (JU) through the project eFlows4HPC (grant agreement No 955558). The JU receives support from the European Union Horizon 2020 research and innovation program and Spain, Germany, France, Italy, Poland, Switzerland, Norway. This publication is also part of the R&D project PCI2021-121944, financed by MCIN/AEI/10.13039/501100011033 and by the ‘‘European Union NextGenerationEU/PRTR’’. The authors also acknowledge financial support from the Spanish Ministry of Economy and Competitiveness, through the ‘‘Severo Ochoa Programme for Centres of Excellence in R&D’’ (CEX2018-000797-S).

Guglielmo Scovazzi was supported by the Army Research Office, United States (ARO) under Grant W911NF-18-1-0308, the National Science Foundation, United States under Grant 2207164 (Division of Mathematical Sciences – DMS), and by Lawrence Livermore National Laboratory, United States under an LDRD Grant.

Claudio Canuto performed this research with the support of the Italian MIUR PRIN Project 201752HKH8-003. He is a member of the Italian INdAM-GNCS research group.

Antonio Rodríguez-Ferran was supported by the Spanish Ministry of Science and Innovation (grant PID2020-116141GB-I00).

Appendix. Some useful inequalities

Hereafter, we collect some well-known inequalities that are used in the mathematical proof of Section 3.

Theorem 4 (Trace Theorem). *Assume $A \subset \mathbb{R}^{n_d}$ is open and bounded and ∂A is Lipschitz. Then the trace operator $T : H^1(A) \rightarrow L^2(\partial A)$ such that $Tw = w|_{\partial A}$ satisfies*

$$\|w\|_{L^2(\partial A)}^2 = \|Tw\|_{L^2(\partial A)}^2 \leq C \left(l(A)^{-1} \|w\|_{0,A}^2 + l(A) |w|_{1,A}^2 \right), \quad \forall w \in H^1(A), \quad (\text{A.1})$$

where C is a constant that may depend on the shape of A but not on its size, and $l(A) = \text{meas}(A)^{1/n_d}$ is a characteristic length of the domain A .

Let $\tilde{\mathcal{T}}^h$ be the regular triangulation introduced in Section 2.1, and let $H^k(\tilde{\Omega}_h, \tilde{\mathcal{T}}^h) = \prod_{T \in \tilde{\mathcal{T}}^h} H^k(T)$ be the ‘broken’ Sobolev space of order $k \geq 0$ with semi-norm $|v|_{k, \tilde{\Omega}_h, \tilde{\mathcal{T}}^h} = \sum_{T \in \tilde{\mathcal{T}}^h} |v|_{k,T}$. For the sake of simplicity, here and in the rest of the paper we use the symbol $|hv|_{k, \tilde{\Omega}_h, \tilde{\mathcal{T}}^h}$ to indicate the scaled quantity $\sum_{T \in \tilde{\mathcal{T}}^h} |h_T v|_{k,T}$. The general trace theorem above can be particularized to functions belonging to such spaces as follows.

Theorem 5 (Scaled Trace Inequalities). *There exists a constant $c_I > 0$ independent of the mesh size such that for any element $T \subset \tilde{\Omega}_h$ with an edge $\gamma_T \subset \tilde{\Gamma}_h$ one has*

$$\|h_T^{1/2} w\|_{0, \gamma_T}^2 \leq c_I \left(\|w\|_{0,T}^2 + |h_T w|_{1,T}^2 \right), \quad \forall w \in H^1(T). \quad (\text{A.2a})$$

Summing over all the elements with at least one of their edges on the boundary $\tilde{\Gamma}_h$, we obtain

$$\|h^{1/2} w\|_{0, \tilde{\Gamma}_h}^2 \leq c_I \left(\|w\|_{0, \tilde{\Omega}_h}^2 + |hw|_{1, \tilde{\Omega}_h, \tilde{\mathcal{T}}^h}^2 \right), \quad \forall w \in H^1(\tilde{\Omega}_h, \tilde{\mathcal{T}}^h). \quad (\text{A.2b})$$

Combining these inequalities component-wise, one gets analogous results for vector- or tensor-valued functions.

Theorem 6 (Scaled Vector/Tensor Trace Inequalities). *There exists a constant $C_I > 0$ independent of the mesh size such that*

$$\|h_T^{1/2} \nabla w \cdot \mathbf{v}\|_{0, \gamma_T}^2 \leq C_I \left(|w|_{1,T}^2 + |h_T w|_{2,T}^2 \right), \quad \forall w \in H^2(T), \quad (\text{A.3a})$$

$$\|h^{1/2} \nabla w \cdot \mathbf{v}\|_{0, \tilde{\Gamma}_h}^2 \leq C_I \left(|w|_{1, \tilde{\Omega}_h}^2 + |hw|_{2, \tilde{\Omega}_h, \tilde{\mathcal{T}}^h}^2 \right), \quad \forall w \in H^1(\tilde{\Omega}_h) \cap H^2(\tilde{\Omega}_h, \tilde{\mathcal{T}}^h), \quad (\text{A.3b})$$

$$\begin{aligned} \|h^{1/2} \boldsymbol{\varepsilon}(w) \tilde{\mathbf{n}}\|_{0, \tilde{\Gamma}_h}^2 &\leq C_I \left(\|\boldsymbol{\varepsilon}(w)\|_{0, \tilde{\Omega}_h}^2 + |h\boldsymbol{\varepsilon}(w)|_{1, \tilde{\Omega}_h, \tilde{\mathcal{T}}^h}^2 \right) \\ &\leq C_I \left(|w|_{1, \tilde{\Omega}_h}^2 + |hw|_{2, \tilde{\Omega}_h, \tilde{\mathcal{T}}^h}^2 \right), \quad \forall w \in (H^1(\tilde{\Omega}_h) \cap H^2(\tilde{\Omega}_h, \tilde{\mathcal{T}}^h))^{n_d}. \end{aligned} \quad (\text{A.3c})$$

In (A.3a) and (A.3b), \mathbf{v} denotes any unit vector field defined on the boundary.

Using the equivalence of norms in a finite dimensional space, we obtain the following trace inequalities for piecewise-affine functions.

Theorem 7 (Discrete Trace Inequalities). *There exist constants $\tilde{c}_I, \tilde{C}_I > 0$ independent of the mesh size, such that*

$$\|\sqrt{h_T} w\|_{0,\gamma_T}^2 \leq \tilde{c}_I \|w\|_{0,T}^2, \quad \forall w \in \mathcal{P}^1(T), \quad (\text{A.4a})$$

and, for all vector functions \mathbf{w}^h belonging to the space of piecewise-linear and globally continuous functions over the mesh $\tilde{\mathcal{T}}$,

$$\|h^{1/2} \nabla \mathbf{w}^h \cdot \mathbf{v}\|_{0,\tilde{\Gamma}_h}^2 \leq \tilde{C}_I \|\nabla \mathbf{w}^h\|_{0,\tilde{\Omega}_h}^2, \quad (\text{A.4b})$$

$$\|\sqrt{h} \nabla \cdot \mathbf{w}^h\|_{0,\tilde{\Gamma}_h}^2 \leq \tilde{C}_I \|\nabla \cdot \mathbf{w}^h\|_{0,\tilde{\Omega}_h}^2, \quad (\text{A.4c})$$

$$\|h^{1/2} \varepsilon(\mathbf{w}^h) \tilde{\mathbf{n}}\|_{0,\tilde{\Gamma}_h}^2 \leq \tilde{C}_I \|\varepsilon(\mathbf{w}^h)\|_{0,\tilde{\Omega}_h}^2. \quad (\text{A.4d})$$

In the second inequality, \mathbf{v} denotes any unit vector field defined on the boundary.

References

- [1] Daniele Boffi, Lucia Gastaldi, A finite element approach for the immersed boundary method, *Comput. Struct.* 81 (8) (2003) 491–501.
- [2] Erik Burman, Ghost penalty, *C. R. Math.* 348 (21–22) (2010) 1217–1220.
- [3] Anita Hansbo, Peter Hansbo, An unfitted finite element method, based on Nitsche's method, for elliptic interface problems, *Comput. Methods Appl. Mech. Engrg.* 191 (47) (2002) 5537–5552.
- [4] B. Schott, U. Rasthofer, V. Gravemeier, W.A. Wall, A face-oriented stabilized Nitsche-type extended variational multiscale method for incompressible two-phase flow, *Internat. J. Numer. Methods Engrg.* 104 (7) (2015) 721–748.
- [5] Erik Burman, Peter Hansbo, Mats Larson, A cut finite element method with boundary value correction, *Math. Comp.* 87 (310) (2018) 633–657.
- [6] Erik Burman, Peter Hansbo, Mats G. Larson, Dirichlet boundary value correction using Lagrange multipliers, 2019.
- [7] Erik Burman, Peter Hansbo, Mats G. Larson, A cut finite element method with boundary value correction for the incompressible Stokes equations, in: *European Conference on Numerical Mathematics and Advanced Applications*, Springer, 2017, pp. 183–192.
- [8] Erik Burman, Peter Hansbo, Fictitious domain finite element methods using cut elements: I. A stabilized Lagrange multiplier method, *Comput. Methods Appl. Mech. Engrg.* 199 (41–44) (2010) 2680–2686.
- [9] Erik Burman, Peter Hansbo, Fictitious domain finite element methods using cut elements: II. A stabilized Nitsche method, *Appl. Numer. Math.* 62 (4) (2012) 328–341.
- [10] Erik Burman, Miguel A. Fernández, An unfitted Nitsche method for incompressible fluid–structure interaction using overlapping meshes, *Comput. Methods Appl. Mech. Engrg.* 279 (2014) 497–514.
- [11] Erik Burman, Daniel Elfverson, Peter Hansbo, Mats G. Larson, Karl Larsson, Shape optimization using the Cut Finite Element Method, *Comput. Methods Appl. Mech. Engrg.* 328 (2018) 242–261.
- [12] André Massing, Mats Larson, Anders Logg, Marie Rognes, A Nitsche-based cut finite element method for a fluid–structure interaction problem, *Commun. Appl. Math. Comput. Sci.* 10 (2) (2015) 97–120.
- [13] Erik Burman, Susanne Claus, Peter Hansbo, Mats G. Larson, André Massing, CutFEM: Discretizing geometry and partial differential equations, *Internat. J. Numer. Methods Engrg.* 104 (7) (2015) 472–501.
- [14] David Kamensky, Ming-Chen Hsu, Yue Yu, John A. Evans, Michael S. Sacks, Thomas J.R. Hughes, Immersogeometric cardiovascular fluid–structure interaction analysis with divergence-conforming B-splines, *Comput. Methods Appl. Mech. Engrg.* 314 (2017) 408–472.
- [15] Fei Xu, Dominik Schilling, David Kamensky, Vasco Varduhn, Chenglong Wang, Ming-Chen Hsu, The tetrahedral Finite Cell Method for fluids: Immersogeometric analysis of turbulent flow around complex geometries, *Comput. & Fluids* 141 (2016) 135–154.
- [16] Santiago Badia, Francesc Verdugo, Alberto F. Martín, The aggregated unfitted finite element method for elliptic problems, *Comput. Methods Appl. Mech. Engrg.* 336 (2018) 533–553.
- [17] Rubén Zorrilla, Antonia Larese, Riccardo Rossi, A modified finite element formulation for the imposition of the slip boundary condition over embedded volumeless geometries, *Comput. Methods Appl. Mech. Engrg.* 353 (2019) 123–157.
- [18] Rubén Zorrilla, Antonia Larese, Riccardo Rossi, A discontinuous nitsche-based finite element formulation for the imposition of the Navier–slip condition over embedded volumeless geometries, *Internat. J. Numer. Methods Fluids* 93 (9) (2021) 2968–3003.
- [19] Jamshid Parvizian, Alexander Düster, Ernst Rank, Finite Cell Method, *Comput. Mech.* 41 (1) (2007) 121–133.
- [20] Alexander Düster, Jamshid Parvizian, Zhengxiong Yang, Ernst Rank, The Finite Cell Method for three-dimensional problems of solid mechanics, *Comput. Methods Appl. Mech. Engrg.* 197 (45) (2008) 3768–3782.
- [21] Klaus Höllig, *Finite Element Methods with B-Splines*, SIAM, Philadelphia, 2003.
- [22] Klaus Höllig, Ulrich Reif, Joachim Wipper, Weighted extended B-spline approximation of Dirichlet problems, *SIAM J. Numer. Anal.* 39 (2) (2001) 442–462.
- [23] T. Rübberg, F. Cirak, Subdivision-stabilised immersed B-spline finite elements for moving boundary flows, *Comput. Methods Appl. Mech. Engrg.* 209 (2012) 266–283.
- [24] T. Rübberg, F. Cirak, A fixed-grid B-spline finite element technique for fluid–structure interaction, *Internat. J. Numer. Methods Fluids* 74 (9) (2014) 623–660.
- [25] Alexei Lozinski, A new fictitious domain method: Optimal convergence without cut elements, *C. R. Math.* 354 (7) (2016) 741–746.
- [26] Alex Main, Guglielmo Scovazzi, The Shifted Boundary Method for embedded domain computations. Part I: Poisson and Stokes problems, *J. Comput. Phys.* 372 (2018) 972–995.
- [27] James H. Bramble, Todd Dupont, Vidar Thomée, Projection methods for Dirichlet's problem in approximating polygonal domains with boundary-value corrections, *Math. Comp.* 26 (120) (1972) 869–879.
- [28] James H. Bramble, J. Thomas King, A finite element method for interface problems in domains with smooth boundaries and interfaces, *Adv. Comput. Math.* 6 (1) (1996) 109–138.
- [29] James H. Bramble, J. Thomas King, A robust finite element method for nonhomogeneous Dirichlet problems in domains with curved boundaries, *Math. Comp.* 63 (207) (1994) 1–17.
- [30] Bernardo Cockburn, Manuel Solano, Solving Dirichlet boundary-value problems on curved domains by extensions from subdomains, *SIAM J. Sci. Comput.* 34 (1) (2012) A497–A519.
- [31] Bernardo Cockburn, Weifeng Qiu, Manuel Solano, A priori error analysis for HDG methods using extensions from subdomains to achieve boundary conformity, *Math. Comp.* 83 (286) (2014) 665–699.

- [32] Bernardo Cockburn, Deepa Gupta, Fernando Reitich, Boundary-conforming discontinuous Galerkin methods via extensions from subdomains, *J. Sci. Comput.* 42 (1) (2010) 144.
- [33] Silvia Bertoluzza, Mourad Ismail, Bertrand Maury, The Fat Boundary Method: Semi-discrete scheme and some numerical experiments, in: *Domain Decomposition Methods in Science and Engineering*, Springer, 2005, pp. 513–520.
- [34] Silvia Bertoluzza, Mourad Ismail, Bertrand Maury, Analysis of the fully discrete Fat Boundary Method, *Numer. Math.* 118 (1) (2011) 49–77.
- [35] Roland Glowinski, Tsorng-Whay Pan, Jacques Periaux, A fictitious domain method for Dirichlet problem and applications, *Comput. Methods Appl. Mech. Engrg.* 111 (3–4) (1994) 283–303.
- [36] Alex Main, Guglielmo Scovazzi, The Shifted Boundary Method for embedded domain computations. Part II: Linear advection–diffusion and incompressible Navier–Stokes equations, *J. Comput. Phys.* 372 (2018) 996–1026.
- [37] Ting Song, Alex Main, Guglielmo Scovazzi, Mario Ricchiuto, The shifted boundary method for hyperbolic systems: Embedded domain computations of linear waves and shallow water flows, *J. Comput. Phys.* 369 (2018) 45–79.
- [38] Nabil M. Atallah, Claudio Canuto, Guglielmo Scovazzi, Analysis of the Shifted Boundary Method for the Stokes problem, *Comput. Methods Appl. Mech. Engrg.* 358 (2020) 112609.
- [39] Nabil M. Atallah, Claudio Canuto, Guglielmo Scovazzi, The high-order shifted boundary method and its analysis, *Comput. Methods Appl. Mech. Engrg.* 394 (2022) 114885.
- [40] J. Haydel Collins, Alexei Lozinski, Guglielmo Scovazzi, A penalty-free Shifted Boundary Method of arbitrary order, *Comput. Methods Appl. Mech. Engrg.* 417 (2023) 116301.
- [41] Chuanqi Liu, WaiChing Sun, Shift boundary material point method: an image-to-simulation workflow for solids of complex geometries undergoing large deformation, *Comput. Part. Mech.* 7 (2020) 291–308.
- [42] Nabil M. Atallah, Claudio Canuto, Guglielmo Scovazzi, The shifted boundary method for solid mechanics, *Internat. J. Numer. Methods Engrg.* 122 (20) (2021) 5935–5970.
- [43] Kangan Li, Nabil M. Atallah, Antonio Rodríguez-Ferran, Dakshina M. Valiveti, Guglielmo Scovazzi, The shifted fracture method, *Internat. J. Numer. Methods Engrg.* 122 (22) (2021) 6641–6679.
- [44] Kangan Li, Antonio Rodríguez-Ferran, Guglielmo Scovazzi, A blended shifted-fracture/phase-field framework for sharp/diffuse crack modeling, *Internat. J. Numer. Methods Engrg.* 124 (4) (2023) 998–1030.
- [45] Kangan Li, Antonio Rodríguez-Ferran, Guglielmo Scovazzi, The simple shifted fracture method, *Internat. J. Numer. Methods Engrg.* 124 (2023) 2837–2875.
- [46] Kangan Li, Nabil M. Atallah, G. Alex Main, Guglielmo Scovazzi, The shifted interface method: a flexible approach to embedded interface computations, *Internat. J. Numer. Methods Engrg.* 121 (3) (2020) 492–518.
- [47] Oriol Colomé, Alex Main, Léo Nouveau, Guglielmo Scovazzi, A weighted shifted boundary method for free surface flow problems, *J. Comput. Phys.* 424 (2021) 109837.
- [48] Erik Burman, Peter Hansbo, Mats G. Larson, CutFEM based on extended finite element spaces, *Numer. Math.* 152 (2) (2022) 331–369.
- [49] Nabil Atallah, Claudio Canuto, Guglielmo Scovazzi, Analysis of the shifted boundary method for the Poisson problem in domains with corners, *Math. Comp.* 90 (331) (2021) 2041–2069.
- [50] Alexandre Ern, Jean-Luc Guermond, *Theory and Practice of Finite Elements*, in: *Applied Mathematical Sciences*, vol. 159, Springer New York, 2004.
- [51] J.A. Nitsche, Über ein Variationsprinzip zur Lösung Dirichlet-Problemen bei Verwendung von Teilräumen, die keinen Randbedingungen unterworfen sind, *Abh. Math. Sem. Univ., Hamburg* 36 (1971) 9–15.
- [52] Douglas N. Arnold, Franco Brezzi, Bernardo Cockburn, L. Donatella Marini, Unified analysis of discontinuous Galerkin methods for elliptic problems, *SIAM J. Numer. Anal.* 39 (5) (2002) 1749–1779.
- [53] Alexei Lozinski, CutFEM without cutting the mesh cells: A new way to impose Dirichlet and Neumann boundary conditions on unfitted meshes, *Comput. Methods Appl. Mech. Engrg.* 356 (2019) 75–100.
- [54] Thomas J.R. Hughes, Arif Masud, Jing Wan, A stabilized mixed discontinuous Galerkin method for Darcy flow, *Comput. Methods Appl. Mech. Engrg.* 195 (25–28) (2006) 3347–3381.
- [55] Bernard Nayroles, Gilbert Touzot, P38504470764 Villon, Generalizing the finite element method: diffuse approximation and diffuse elements, *Comput. Mech.* 10 (5) (1992) 307–318.
- [56] Nabil M. Atallah, Claudio Canuto, Guglielmo Scovazzi, The second-generation shifted boundary method and its numerical analysis, *Comput. Methods Appl. Mech. Engrg.* 372 (2020) 113341.
- [57] Cheng-Hau Yang, Kumar Saurabh, Guglielmo Scovazzi, Claudio Canuto, Adarsh Krishnamurthy, Baskar Ganapathysubramanian, Optimal surrogate boundary selection and scalability studies for the shifted boundary method on octree meshes, 2023.